AN INVESTIGATION OF A MOVABLE MASS-ATTITUDE STABILIZATION SYSTEM FOR ARTIFICIAL-G SPACE

NASA Contract: NAS8-27952

Final Report

Prepared for
George C. Marshall Space Flight Center
Marshall Space Flight Center, Alabama 35812

Dara W. Childs
Principal Investigator
Associate Professor
of
Mechanical Engineering and
Applied Mathematics
University of Louisville
Louisville, Kentucky

1 November 1972

TABLE OF CONTENTS

NOMENCLATURE

a	$= (I_z - I_y)/I_x$
b	$= (I_z - I_x)/I_y$
b_1	$= (I^1_{z_1} - I^1_{x_1})/I^1_y$
b_2	$= (I^2_{z_2} - I^2_{x_2})/I^2_y$
e	$= I^2_y/I_x$
e_1	$= m_c r^2_y/I_x + m_c r^2_x /I^1_y$
g_2	$= m_c r_y/I_x$
g_1	$= m_c r_x/I^1_y$
I_x, I_y, I_z	= moment of inertias in the x, y, z system of the space station treated as a rigid body
I^1_x, I^1_y, I^1_z	= moment of inertias in the x, y, z system for body 1.
$I^2_{x_2}$, I^2_y , $I^2_{z_2}$	= principal moment of inertias in the x_2, y_2, z_2 system for body 2
$I_{yz}(0)$, $I_{xz}(0)$	= initial product of inertia disturbances for the space station.
k_i	= feedback gains
k_t	= torsional stiffness coefficient for cable connections'
m_c	= control mass magnitude
p_1	= undamped crew-quarter wobble frequency
p_2	= undamped torsional natural frequency
p^2_1	$= (I^1_y + I^2_y)k_t/I^1_y I^2_y$
q_2	$= I^2_y/I_y$
q_1	$= I^1_y/I_y$

r_x, r_y, w	= coordinates of control mass m_c in x, y, z coordinate system
u	= control force
v	= $\dot{w}$
w	= displacement of the control mass m_c (see figure 2).
$\alpha(0)$	= $I_{yz}(0)/(I_z - I_y)$
$\beta(0)$	= $-I_{xz}(0)/(I_z - I_x)$
ζ_i	= damping factor for the ith mode due to feedback control
$\omega_i = p_i(1-\zeta_i^2)^{1/2}$	= imaginary part of the ith feed-back pole
Ω_x, Ω_y	= transverse angular velocity components of the crew quarters
$\overline{\Omega}$	= nominal space station spin velocity
β	= $\dot{\theta}$
θ	= torsional rotation of body 2 relative to body 1.

LIST OF FIGURES

CHAPTER I

INTRODUCTION

1.1 ADMINISTRATIVE INFORMATION

This report covers the work accomplished on NASA contract NAS8-27952 during the time period 1 September 1971 to 1 November 1972 for the George C. Marshall Space Flight Center, Marshall Space Flight Center, Alabama, 35812. The principal investigator for this study was Dr. Dara W. Childs, Associate Professor of Mechanical Engineering, The University of Louisville, Louisville, Kentucky. Inquiries about the results of this study should be directed either to Dr. Childs or Mr. Harry Buchanan (S&E-AERO-R) Marshall Space Flight Center.

1.2 BACKGROUND INFORMATION

The Principal investigator for this study participated in the NASA-ASEE summer faculty program at Marshall Space Flight Center during the summer of 1970. The research topic investigated during this time period was the analysis of a novel "wobble damper" for an artificial-g space station. A space craft is said to be "wobbling" when its axis of maximum moment of inertia is not aligned with its moment-of-momentum vector. This undesirable vehicle motion can be controlled by the use of reaction jets, passive dampers, control moment gyros (CMG's) and momentum wheels. Each of these devices has both advantages and disadvantages, and Dr. Eugene Worley (S&E-AERO-R) suggested the possibility of an active system which would employ a single movable mass to generate

control torques. The stimulus for this proposition was the observation that astronaut motion within the space station (moving masses) would be the principal source of spacecraft wobble motion. It therefore seemed reasonable to assume that controlled motion of a comparable mass could be used to eliminate wobble motion. During the course of the NASA-ASEE summer faculty program, the correctness of this supposition was verified by a combined analytical-simulation study. The results of this study are presented in Reference 1, and demonstrate that a movable mass controller (MMC) represents an extremely attractive alternative for the wobble damping of spacecraft which basically behaves like a rigid body.

The present study was designed to establish the feasibility of an MMC in the attitude stabilization of a cable-connected artificial-g configuration which can not reasonably be idealized as a rigid body. The dynamic model for cable-connected configurations employed in this study accounts for the aggregate motion of the space station and relative torsional motion between the crew quarters and counter weight. The development of the model is the subject of the following chapter.

CHAPTER II

DYNAMIC MODELS

2.1 INTRODUCTION

Most of the past analyses of cable-connected rotating space station configurations have been concerned with (a) the dynamic formulation of the problem, or (b) the stability of the system. Typical dynamic formulations have considered the extensional motion of the system[2,3] or have considered lateral motion of the cables[4,5] with the end bodies assumed to be particles. Stabekis and Bainum[6] have also examined the problem with an extensible cable but consider the end masses to be rigid bodies.

Posnansky and Heeschen[7] have reported the results of an elaborate lumped-parameter simulation of a cable-connected configuration which includes both lateral cable dynamics and rigid-body descriptions for the end bodies. In terms of the present work, their most significant finding was that the fundamental natural frequency of the lateral dynamics (coupled cable and rigid-body motion) was on the order of 1 cps. By comparison, the rigid-body wobble frequency may be on the order of .01 to .1 cps. However, since cables provide comparatively little torsional rigidity, the fundamental torsional frequency may well be below the wobble frequency. From these observed frequency relationships, the dynamic representation derived in this study is based on the following two assumptions:

(a) Lateral and extensional motions are a secondary consideration in designing the attitude-stabilization system, and

(b) Relative roll motion between the end bodies is of central importance in the design of the attitude-stabilization system.

In the sections which follow, a dyamic formulation is derived for the space-station/MMC system based on these assumptions.

2.2 GOVERNING EQUATIONS

Figure 1 illustrates the basic kinematic variables required to define the problem. The X, Y, Z axes define an inertial coordinate system. The x_1, y_1, z_1 and x_2, y_2, z_2 axes are fixed in rigid bodies 1 and 2, respectively, and their origins coincide with the mass centers of these bodies. The x, y, z axes are parallel, respectively, to the x_1, y_1, z_1 axes, and the origin of the x, y, z system coincides with the net mass center of the system. The x_2, y_2, z_2 axes are principal axes for body 2. The angle θ defines the (only) relative motion between the x, y, z (x_1, y_1, z_1) axes and the x_2, y_2, z_2 axes. The vector R locates the origin of the x, y, z system in the X, Y, Z system. The angular velocity of the x, y, z system relative to the X, Y, Z system is defined by the vector Ω, and the angular velocity of the x_2, y_2, z_2 system relative to the x, y, z system is defined by the vector ω.

Body 1 of Figure 1 corresponds to the crew quarters, while body 2 corresponds to the counterweight. By spinning the system about a transverse axis of maximum moment of inertia (nominally the z axis) an artificial-g environment is induced in the crew quarters.

The vectors ρ^1 and ρ^2 denote the position vectors in the x_1, y_1, z_1 and the x_2, y_2, z_2 systems, and the vectors a^1 and a^2 locate the origins of the x_1, y_1, z_1 and x_2, y_2, z_2 systems in the x, y, z systems. Hence, by definition

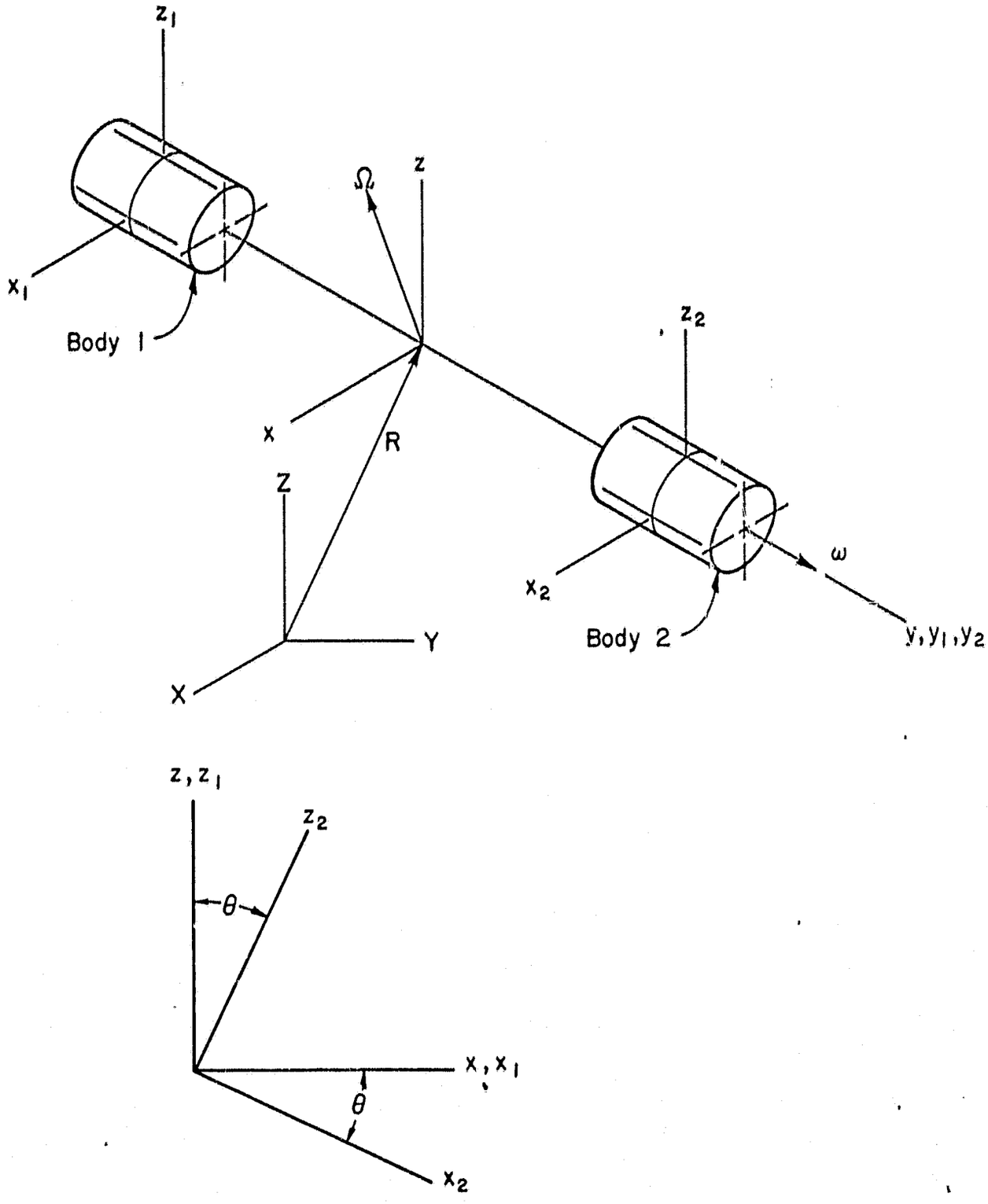

Fig.1 Basic kinematic definitions

$$\int_{m_1} \rho^1 dm = 0 \quad , \quad \int_{m_2} \rho^2 dm = 0 \quad , \quad m_1 a^1 + m_2 a^2 = 0 \tag{1}$$

where m_1 and m_2 are the masses of bodies 1 and 2, respectively.

The following two derivative operations with respect to time are required.

$$\dot{V} = \left.\frac{dV}{dt}\right|_{X,Y,Z} \quad , \quad \hat{\dot{V}} = \left.\frac{dV}{dt}\right|_{x,y,z}$$

where V is an arbitrary vector. The following notation will be used to identify the coordinate system in which the component description of a vector is stated: (V) implies a component description in the x, y, z or x_1, y_1, z_1 system, while $(V)_{i2}$ implies a component description in the x_2, y_2, z_2 system. These vectors are related by the coordinate transformation

$$(V)_{i2} = [\theta](V) = \begin{bmatrix} c\theta & 0 & -s\theta \\ 0 & 1 & 0 \\ s\theta & 0 & c\theta \end{bmatrix} (V) \tag{2}$$

where $s\theta \equiv \sin\theta$, and $c\theta \equiv \cos\theta$.

The first equation employed to define the vectors Ω, ω is

$$\begin{aligned} T^r = & \int_{m_1} (a^1 + \rho^1) \times (\ddot{R} + \ddot{a}^1 + \ddot{\rho}^1)\, dm \\ & + \int_{m_2} (a^2 + \rho^2) \times (\ddot{R} + \ddot{a}^2 + \ddot{\rho}^2)\, dm \end{aligned} \tag{3}$$

where T^r is the resultant external torque applied to the system at the origin of the x, y, z system. By noting the kinematic result

$$\ddot{a}^i = \dot{\Omega} \times a^i + \Omega \times (\Omega \times a^i); \qquad i = 1,2 \tag{4}$$

B

and by introducing Eq. (1), Eq. (3) reduces to

$$T^r = \sum_{i=1}^{2} a^i \times (\dot{\Omega} \times m_i a^i) + \Omega \times \sum_{i=1}^{2} a^i \times (\Omega \times m_i a^j) \tag{5}$$

$$+ \int_{m_1} (\rho^1 \times \ddot{\rho}^1)\, dm + \int_{m_2} (\rho^2 \times \ddot{\rho}^2)\, dm$$

By substituting from the kinematic equations

$$\ddot{\rho}^1 = (\dot{\Omega} \times \rho^1) + \Omega \times (\Omega \times \rho^1) \tag{6}$$

$$\ddot{\rho}^2 = (\dot{\Omega} \times \rho^2) + [(\hat{\dot{\omega}}) + (\Omega \times \omega)] \times \rho^2$$

$$+ (\Omega + \omega) \times [(\Omega + \omega) \times \rho^2],$$

implementing the vector identity $A \times [B \times (B \times A)] = B \times [A \times (B \times A)]$, performing the indicated integrations, and gathering terms, Eq. (5) becomes

$$(T^r) = [J](\dot{\Omega}) + [(\Omega)][J](\Omega) \tag{7}$$

$$+ [J^2](\hat{\dot{\omega}}) + [(\omega)][J^2](\omega)$$

$$+ [J^2](\Omega \times \omega) + [(\omega)][J^2](\Omega) + [(\Omega)][J^2](\omega)$$

where the notation $[(\ )]$ implies

$$[(V)] = \begin{bmatrix} 0 & -V_z & V_y \\ V_z & 0 & -V_x \\ -V_y & V_x & 0 \end{bmatrix}$$

and performs the matrix equivalent of the vector cross-product operation. Returning to Eq. (7), $[J]$ is the inertia matrix for the entire system in the x, y, z coordinate system. Specifically,

$$[J] = [J^1] + [J^2] - \sum_{i=1}^{2} m_i[(a^i)][(a^i)] \tag{8}$$

where $[J^1]$ and $[J^2]$ are the inertia matrices for bodies 1 and 2, (relative to their individual mass centers) in the x, y, z system. The matrix $[J^2]$ is further defined by

$$[J^2] = [\Theta]^T[J^2_{2i}][\Theta] \tag{9}$$

where $[J^2_{2i}]$ is the inertia matrix of body 2 in terms of the x_2, y_2, z_2 system. The last three terms in Eq. (7) can be combined as follows

$$[(d)](\omega) = [J^2](\Omega \times \omega) + [(\omega)][J^2](\Omega) + [(\Omega)][J^2](\omega) \tag{10}$$

where the vector (d) is defined by

$$(d) = \{j[U] - 2[J^2]\}(\Omega) \quad , \quad j = \text{trace } [J^2]. \tag{11}$$

Hence, the final form for Eq. (7) is

$$(T^r) = [J](\dot{\Omega}) + [(\Omega)][J](\Omega) \tag{12}$$
$$+ [J^2](\dot{\omega}) + [(\omega)][J^2](\omega) + [(d)](\omega)$$

The definition of the vectors Ω and ω is completed by the independent equation

$$T^c = \int_{m_2} \rho^2 \times (\ddot{R} + \ddot{a}^2 + \ddot{\rho}^2)\, dm \tag{13}$$

where T^c is the resultant torque applied to body 2 at its mass center. Substituting from Eqs. (1) and (6) into Eq. (13), integrating over m_2, and then substituting from (10) and (11) yields

$$(T^c)_{i2} = [J^2_{i2}](\dot{\Omega})_{i2} + [(\Omega)_{i2}][J^2_{i2}](\Omega)_{i2} \tag{14}$$

$$+ [J^2_{i2}](\dot{\omega})_{i2} + [(\omega)_{i2}][J^2_{i2}](\omega)_{i2} + [(J)_{i2}](\omega)_{i2}$$

Since the x_2, y_2, z_2 axes are principal axes for body 2, the y component of Eq. (14) yields

$$T^c_y = I^2_y \dot{\Omega}_y + I^2_y \ddot{\theta} + (I^2_{z2} - I^2_{x2})\{(\Omega^2_z - \Omega^2_x)s\theta c\theta - \Omega_x\Omega_z c(2\theta)\} \tag{15}$$

where I^2_{x2}, I^2_y, I^2_{z2} are the moments of inertia for body 2 relative to the x_2, y_2, z_2 principal axes, respectively. Further, Ω_x, Ω_y, Ω_z are the components of Ω in the x, y, z system. Eq. (15) and the matrix equation (12) define the uncontrolled motion of the system. The assumption is made in this study that T^c_y is the reaction torque defined by

$$T^c_y = - k_t\theta \tag{16}$$

where k_t is a torsional spring constant.

Figure 2 illustrates the MMC system to be used in this study. The essential element of the stabilizer is the point mass m_c whose motion is limited by a tube (or other physical constraints) to be parallel with the z axis. The tube is attached to body 1, and the position of the mass within the tube is defined by the variable w. The governing equation of motion for w is[3]

$$f_z = m_c\{\ddot{w} + (\dot{\Omega}_x r_y - \dot{\Omega}_y r_x) + r_x\Omega_z\Omega_x \tag{17}$$

$$+ r_y\Omega_z\Omega_y - w(\Omega^2_x + \Omega^2_y)\}$$

where f_z is the z component of the reaction force applied to m_c, and

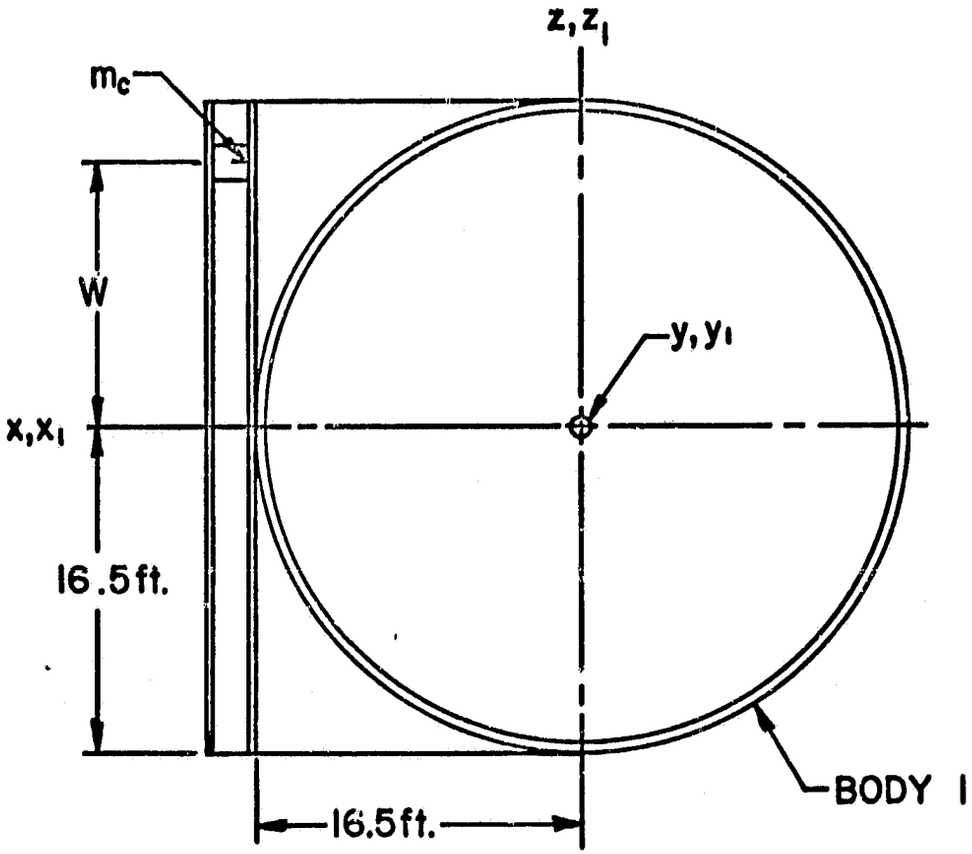

Fig. 2 Controller configuration

(r_x, r_y, w) are the components of r, the vector which locates the control mass in the x, y, z system.

The attachment of the MMC system to body 1 as illustrated in Fig. 2 will only change Eq. (12). The required modification is

$$(T^r) = [\bar{J}](\dot{\Omega}) + [(\Omega)][\bar{J}](\Omega) + [J^2](\hat{\dot{\omega}}) + [(\omega)][J^2](\omega) + [(d)](\omega) + m_c[(r)](\hat{\ddot{r}}) + 2m_c[(r)][(\Omega)](\hat{\dot{r}}) \tag{18}$$

where

$$[\bar{J}] = [J] - m_c[(r)][(r)] \tag{19}$$

Summarizing, the variables $(\Omega_x, \Omega_y, \Omega_z, \theta, w)$ are defined by Eqs. (15), (17), and (18).

From Eq. (19), the inertia matrix $[\bar{J}]$ is seen to be a function of both w and θ. Of particular importance are the relationships

$$\bar{I}_{xz} = I_{xz}(0) + m_c r_x w - (I_{z2}^2 - I_{x2}^2)s\theta c\theta$$
$$\bar{I}_{yz} = I_{yz}(0) + m_c r_y w \tag{20}$$

2.3 UNCONTROLLED MOTION: LINEARIZED MODEL

The free motion dynamics problem can be summarized as follows. Under ideal conditions, the H (moment-of-momentum) vector and the axis of maximum moment of inertia of the spacestation coincide. If (due to either external torques or internal mass motion) the two are forced apart, a condition generally called "wobbling" results. This motion is characterized by a nominally constant rotation rate about the z axis accompanied by oscillations in Ω_x, Ω_y, and θ.

The defining equations for free motion are Eqs. (12) and (15), and a valid linearization of these equations is possible based on the following observations:

(a) $\Omega_z \approx \bar{\Omega}$, the average spin velocity,

(b) Ω_x and Ω_y are very small in comparison to $\bar{\Omega}$, and

(c) θ is generally small justifying the approximations $c\theta = 1$, $s\theta = \theta$.

The resultant linearized equations are

$$\begin{aligned} \dot{\Omega}_x &= -\Omega_y a\bar{\Omega} + \dot{\theta} e(1-b_2)\bar{\Omega} - a\bar{\Omega}^2 \alpha(0) \\ \dot{\Omega}_y &= \Omega_x b_1\bar{\Omega} + (k_t/I_y^1)\theta - b\bar{\Omega}^2 \beta(0)/q_1 \\ \ddot{\theta} &= -\Omega_x(b-b_2)\bar{\Omega}/q_1 - (P_1^2+b_2\bar{\Omega}^2)\theta + b\bar{\Omega}^2\beta(0)/q_1 \end{aligned} \tag{21}$$

where the result, $b_1 = (b-q_2b_2)/q_1$, is employed . Two special cases can be obtained from these general results. First, if $k_t \to \infty$, θ and $\dot{\theta} \to 0$, $q_1 \to 1$, and $b_1 \to b$. The result is the rigid body equations.

$$\begin{aligned} \dot{\Omega}_x &= -\Omega_y a\bar{\Omega} - a\bar{\Omega}^2 \alpha(0) \\ \dot{\Omega}_y &= \Omega_x b\bar{\Omega} - b\bar{\Omega}^2 \beta(0) \end{aligned} \tag{22}$$

with the rigid-body wobble frequency

$$p = (ab)^{1/2}\,\bar{\Omega} \tag{23}$$

The second special case results if $k_t = b_2 = 0$. Since $e = I_y^2/I_x$ is in general quite small, the resultant motion is approximately defined by

$$\dot{\Omega}_x = -\Omega_y a\bar{\Omega} - a\bar{\Omega}^2\beta\,(0)$$

$$\dot{\Omega}_y = \Omega_x b_1\bar{\Omega} - b\bar{\Omega}^2\beta\,(0)/q_1 \qquad (24)$$

$$\ddot{\theta} = -\Omega_x b_1\bar{\Omega} - b_2\bar{\Omega}^2\theta + b\bar{\Omega}^2\beta\,(0)/q$$

The "rigid body" wobble frequency and the torsional oscillation frequency p_2 are defined by

$$p_1 = \{a\ b_1\}^{1/2}\ \bar{\Omega}\ ,\ p_2 = b_2^{1/2}\ \bar{\Omega} \qquad (25)$$

2.4 CONTROLLED MOTION:LINEARIZED MODEL

As stated previously, motion of the complete system is defined by Eqs. (15), (17), and (18). A valid linearization of the controlled system is possible based on the preceding assumptions for free motion ($\Omega_z \cong \bar{\Omega}$; Ω_x, $\Omega_y << \bar{\Omega}$; $s\theta \cong \theta$, $c\theta \cong 1$) plus the following assumptions for the MMC:

(a) $m_c w^2/I_x << 1$, $m_c w^2/I_y << 1$, and

(b) the "coriolis-torques" $2m_c w\dot{w}\Omega_x$ and $2m_c w\dot{w}\Omega_y$ which arise in Eq. (18) due to the term $2m_c\,[(r)][(\Omega)](\dot{r})$ are negligible.

The resultant linearized equations may be written as

$$\begin{Bmatrix} \dot{\Omega}_x \\ \dot{\Omega}_y \\ \dot{\beta} \\ \dot{\theta} \\ \dot{v} \\ \dot{w} \end{Bmatrix} = \begin{bmatrix} 0 & -\bar{\Omega}a & \bar{\Omega}a(1-b_2) & 0 & 0 & -\bar{\Omega}^2 g_2 \\ \bar{\Omega}b & 0 & 0 & k_t/I_y^1 & 0 & \bar{\Omega}^2 g_1 \\ -\bar{\Omega}(b-b_2)/q_1 & 0 & 0 & -(b_2\bar{\Omega}^2+P_1^2) & 0 & -\bar{\Omega}^2 g_1 \\ 0 & 0 & 1 & 0 & 0 & 0 \\ \bar{\Omega}r_x(b_1-1) & \bar{\Omega}r_y(a-1) & -\bar{\Omega}r_y e(1-b_2) & r_x k_t/I_y^1 & 0 & \bar{\Omega}^2 e_1 \\ 0 & 0 & 0 & 0 & 1 & 0 \end{bmatrix} \begin{Bmatrix} \Omega_x \\ \Omega_y \\ \beta \\ \theta \\ v \\ w \end{Bmatrix}$$

$$+ \begin{Bmatrix} -r_y/I_x \\ r_x/I^1_y \\ -r_x/I^1_y \\ 0 \\ (1+e_1)/m_c \\ 0 \end{Bmatrix} u + \bar{\Omega}^2 \begin{Bmatrix} -a\alpha(0) \\ -b\beta(0)/q_1 \\ b\beta(0)/q_1 \\ 0 \\ r_y a\alpha(0) - r_x b\beta(0)/q_1 \\ 0 \end{Bmatrix} \qquad (26)$$

In the equation above, u is the control contribution to the force f_z appearing in Eq. (17). A comparison between the solutions from this linear model with those of the general non-linear model (Eqs. (18), (17), and (15)) for a wide range of cases revealed no significant differences, In most cases no discernible differences were evident in plots of the solutions.

CHAPTER III

DATA, AGREEMENTS, AND ASSUMPTIONS

3.1 CONTROL OBJECTIVES AND CONTRAINTS

The general attitude-stabilization control objectives may be defined in terms of the control force u and the state-variable vector X (Ω_x, Ω_y, β, θ, v, w). In terms of these variables, the basic requirement is the synthesis of a feedback control logic u = u(X) which satisfies the following descending order of objectives:

(a) The attitude-stabilization system is required to eliminate the oscillations in the transverse angular velocity components of body 1 (Ω_x, Ω_y), i.e., the desired terminal state is $\dot{\Omega}_x(t_f) = \dot{\Omega}_y(t_f) = 0$.

(b) While the comfort of the astronauts does not explicitly depend on $\dot{\theta}$ also being forced to zero, the coupling of the system is such that condition (a) cannot generally ($k_t \neq 0$) be otherwise satisfied. Hence, an additional desired terminal state is $\dot{\theta}(t_f) = 0$.

(c) It is desirable that the full capacity of the controller be restored after a disturbance has been eliminated, hence, the additional desired terminal states $w(t_f) = \dot{w}(t_f) = 0$.

In summary, the desired terminal state is

$$\dot{\Omega}_x(t_f) = \dot{\Omega}_y(t_f) = \dot{\theta}(t_f) = w(t_f) = \dot{w}(t_f) = 0 \qquad (27)$$

The control constraints can be summarized as follows:

(a) Motion of the control mass is amplitude limited by physical constraints, i.e.,

$$|w| \leq W = 16.5 \text{ ft.} \tag{28}$$

(b) A control which requires an excessive control force u is deemed to be impractical. Specifically, in this study control forces in excess of thirty-five pounds were deemed to be unacceptable; hence,

$$|u| \leq U = 35 \text{ lbs.} \tag{29}$$

In addition to these specific and easily quantifiable requirements and constraints, the feedback control logic to be derived was constrained to be time-invariant and (generally) linear in form. Specifically, a control law of the form

$$u = k_1\Omega_x + k_2\Omega_y + k_3\dot{\theta} + k_4\theta + k_5\dot{w} + k_6 w + k_7\int_0^t w(\tau)d\tau \tag{30}$$

was employed where the integral term was added for the sole purpose of enforcing the terminal boundary condition $w(t_f) = 0$, and has no other intended influence on the dynamics of the system.

From Eqs. (26) and (30), the control system has the form

$$\dot{X} = AX + bu + f \ , \ u = k^T X \tag{31}$$

or in closed-loop form

$$\dot{X} = [A + bk^T] X + f \tag{32}$$

In general terms, the control synthesis problem addressed here can be stated as follows. Determine those gains k_i which will cause the controlled system defined by Eq. (32) to rapidly recover from an initial disturbance, and to approach the desired terminal state given in Eq. (27) without violating the constraints of Eqs. (28) and (29).

3.2 SPACE-STATION CONFIGURATIONS AND DATA

To this investigator's knowledge, NASA's more recent investigation of artificial-g space stations have concentrated on the following three concepts:

(a) A nuclear-powered, nominally axisymmetric configuration for which two bodies are connected by a comparatively rigid connecting tunnel,

(b) A nuclear-powered, nominally axisymmetric configuration for which two bodies are connected by cables, and

(c) A solar-powered, axymmetric cable-connected configuration.

Concepts (a) and (b) were investigated by McDonnell-Douglas Astronautics company under the direction of Marshall Space Flight Center, while concept (c) was investigated by North American-Rockwell under the direction of The Manned Space Flight Center, NASA Houston.

The superior performance of an MMC for attitude stabilization of concept (a) has previously been demonstrated in Reference 1, and the investigations of this study are restricted to concept (b). Specifically, the configuration investigated in this study is based on the geometric and inertial properties arrived at by McDonnell-Douglas Astronautics in Reference 8. Table A illustrates the significant longitudinal dimensions of this space station design in its various stages of deployment.

The inertia properties for the space station in its various stages of deployment are provided in Table B. The asymmetry which is evident (i.e., $I_Z > I_X$, $I_Z^1 > I_X^1$, $I_Z^2 > I_X^2$) in this table was added by the investigators to the nominal symmetric properties provided by Reference 8. The following guidelines were used to arrive at these modified inertial properties:

TABLE A: AXIAL SPACE-STATION DIMENSIONS

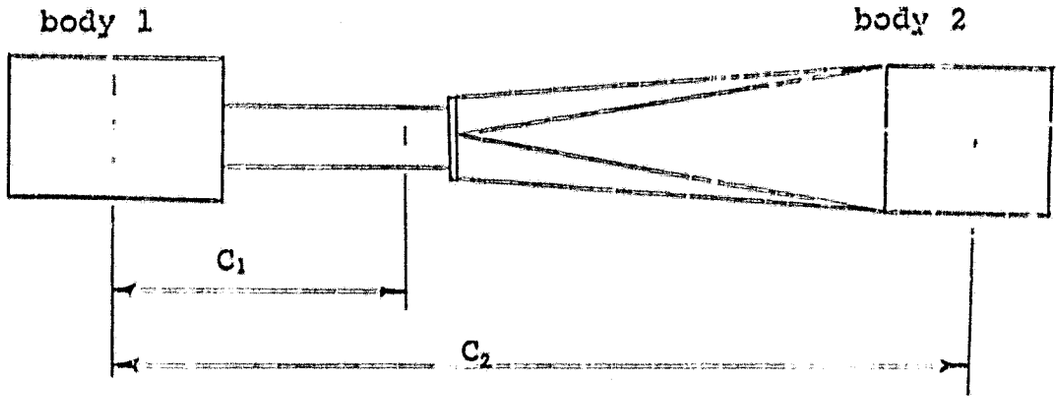

Deployment Stage	C_1	C_2	Cable Length	r_y
0	57.16	166.2	0.0	-51.5
1/4	69.28	201.4	35.3	-63.6
1/2	81.41	236.7	70.5	- 75.8
3/4	93.53	272.0	105.8	- 87.9
1	105.7	307.2	141.0	-100.0

C_1 (ft) = distance from C.M. of body 1 to C.M. of space station

C_2 (ft) = distance from C.M. of body 1 to C.M. of body 2

r_y (ft) = distance from C.M. of space station to MMC

(a) Dynamic stability of the system requires asymmetry.

(b) The crew quarters are nominally axisymmetric, and the provision of asymmetry requires additional design effort and expense. The assumption was made that asymmetry would be provided by the internal mass-distribution design of the crew quarters, and the asymmetry used in Reference 1 was taken to be representative of the degree of asymmetry which

could be obtained by this approach.

(c) The counterweight is also nominally axisymmetric, and it turns out that (from a controls viewpoint) a perfectly axisymmetric body is ideal. Consequently, sufficient asymmetry was provided in body 2 to account for residual (but unintentional) counterweight asymmetry.

3.3 REFERENCE DISTURBANCES AND CONTROLLER SIZING

The reference disturbance used throughout this study consists of four astronauts (773 lbs. or 24 slugs) moved instantaneously to the worst possible locations within the crew quarters. The resultant initial product-of-inertia disturbances for the fully deployed configuration are

$$I_{xz}(0) = 3250 \text{ slug-ft}^2, \quad I_{yz}(0) = 51{,}000 \text{ slug-ft}^2 \tag{33}$$

These product-of-inertias were used for all stages of deployment.

Eq. (20) demonstrates the linear dependence of the I_{xz} and I_{yz} product of inertias upon the controller position w, and it is primarily through this dependence that the MMC system is used to generate control torques. The MMC considered in this study is defined by the parameters

$$r_x = 16.5 \text{ ft.}, \quad m_c = 11 \text{ slugs} \tag{34}$$

The parameter r_y depends upon the stage of deployment and is defined in Table A. The product-of-inertia capacity of the controller is from Eqs. (20) and (28) $I^c_{xz} = 3000$ slug-ft^2, $I^c_{yz} = 18{,}200$ slug-ft^2 ($r_y = 100$ ft). The equivalent static torque capability (for $\bar{\Omega} = 4$ rpm, and $r_y = 100$ ft.) is approximately $|T_x|_{max} = |I^c_{yz}|\bar{\Omega}^2 = 3180$ ft-lbs, and $|T_y|_{max} = |I^c_{xz}|\bar{\Omega}^2 = 525$ ft-lbs. Since

TABLE B: INERTIA PROPERTIES AND PARAMETERS

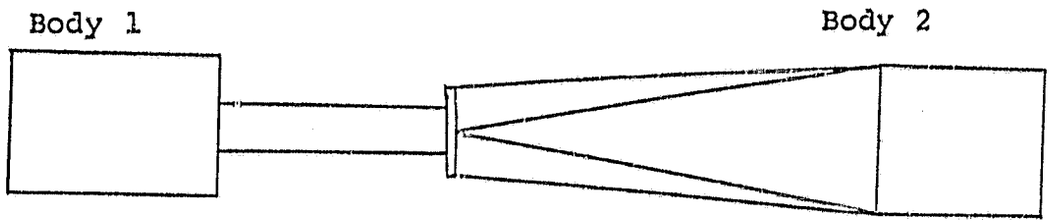

Deployment Stage	I_x (slug-ft^2)	I_y (slug-ft^2)	$\dot{a}$
0	64.926×10^6	65.009×10^6	.9796
1/4	90.166×10^6	90.249×10^6	.9853
1/2	119.91×10^6	119.99×10^6	.9889
3/4	154.13×10^6	154.21×10^6	.9914
1	187.10×10^6	187.18×10^6	.9929

Constant Inertial Parameters

$I_y^1 = .621 \times 10^6$ slug-ft^2

$I_y^2 = .787 \times 10^6$ slug-ft^2

$I_y = 1.407 \times 10^6$ slug-ft^2

$b_2 = .0500$, $b_1 = .0709$, $b = .0592$

the products of inertias are linear functions of w, the control torques may be varied linearly from zero to full capacity.

3.4 DEPLOYMENT AND RETRACTION PROCEDURES

The assumption was made in this study that the nominal design spin velocity $\bar{\Omega}$ is 4 rpm, and that in both the deployment and

retraction phases the spin-velocity could only exceed this value. In other words, the rigidly assembled space station would be over spun prior to deployment. As deployment proceeded, the spin-velocity would drop (conservation of angular momentum), and when fully deployed would rotate at 4 rpm. Basically the same procedure would be followed in the retraction phase. Hence, spin velocities of 4 rpm and higher were investigated. This approach was found to be conservative, since in general increasing the spin-velocity degrades the controller's performance.

3.5 TORSIONAL STIFFNESS COEFFICIENTS

The two following configurations were used in defining the torsional stiffness k_t:

(a) a zero torsional stiffness configuration ($k_t = 0$), corresponding to a single cable design, and

(b) a maximum torsional stiffness configuration corresponding to the McDonnell-Douglas design.

The relatively high torsional stiffness of the McDonnell-Douglas design was verified by simulations (at MSFC) of alternative designs. The calculation of the values for k_t were based on the work of D. Nixon[9] (S&E-AERO-R), and were aided by personal communications with Mr. Nixon.

3.6 SYNTHESIS PROCEDURE

One important feature of the state variable formulation of a linear feedback control system is the fact that the poles of the closed-loop transfer function can be positioned arbitrarily by the proper choice of feedback gains (if all the state

variables are available). The closed loop characteristic equation of a system written in the form $\dot{X} = [A+bk^T]X$ is given by the determinant $|sI - A - bk^T|$. For an nth order system, the characteristic equation is an nth order polynomial in the Laplacian operator s, with n + 1 terms. The coefficient of the s^n term equals one, and the coefficients of the s^{n-1} to s^0 terms provide n algebraic equations in terms of the n unknown feedback gains k_i that can be equated to the corresponding coefficients of any desired nth order characteristic polynomial. By solving this set of n equations, the closed-loop poles of the system can be positioned to obtain desired frequency domain solutions.

The effectiveness of the root specification method as a control system design technique is limited by the fact that the transient magnitudes of the various system and control variables cannot be predicted from frequency-domain solutions. Two major constraints imposed on the performance of the control system considered in this study were a maximum control mass deflection magnitude, (Eq. (28)) and a maximum control force magnitude (Eq. (29)). While the ability to calculate feedback gains to yield desired degrees of damping on the system variables is of considerable use, intuitions based on past experiences and trial and error procedures provide the only insight into the effect of pole locations upon the maximum variable magnitudes in time domain solutions. In this phase of the study, gains were first calculated to yield roots specified from physical and intuitive bases. Time responses using these gains were then obtained by numerical inte-

gration of the system's equations of motion to determine whether the gains caused the system constraints to be violated.

The method of closed-loop pole specification was applied to both the fourth-order, non-deployed rigid body configuration and the sixth-order, cable connected configuration of Eq. (26). The characteristic equations of the two systems were established by expanding the determinant of the closed-loop system coefficient matrix. The closed-loop characteristic polynomial for the cable-connected system is provided in Appendix A. Sets of equations relating the unknown feedback gains to the desired closed-loop poles were obtained by equating the coefficients of the closed-loop polynomial to those of the desired characteristic equation. A computer program utilizing the IBM Scientific Subroutine Package program, SIMQ, was developed to solve the equation sets. Two additional IBM subroutines, HSBG and ATEIG, were used to calculate the eigenvalues of the closed-loop system matrix for each set of calculated gains to verify that the desired roots were actually obtained.

The general criteria for selecting desired root locations can be explained as follows. First, one notes from Eq. (26) that without control the control mass motion is itself unstable due to the coefficient $A_{56} = \bar{\Omega}^2 e_1$. Assuming that the controller is stabilized (via the $k_6 w$ term in Eq. (30) with all other $k_i = 0$), the system defined by Eq. (26) has the following three undamped modes of motion and natural frequencies:

(a) wobble motion involving Ω_x and Ω_y (natural frequency = p_1),

(b) torsional motion involving β and θ (natural frequency = p_2), and

(c) control mass motion involving v and w (natural frequency $= p_3$).

Hence, the characteristic equation for the uncontrolled system has the form

$$\prod_{i=1}^{3} (s^2 + p_i^2) = 0 \tag{35}$$

The gains k_i are selected so that the closed-loop characteristic equation has the form

$$(s + p_0) \prod_{i=1}^{3} (s^2 + 2\zeta_i p_i s + p_i^2) = 0 \tag{36}$$

where the $s + p_0$ term arises due to the integral feedback term. The damping factor for wobble motion ζ_1 was selected to be unity in all cases. The damping factors for the control mass and torsional motion were selected to yield equivalent damping constants, i.e., $\zeta_1 p_1 = \zeta_2 p_2 = \zeta_3 p_3$. The natural frequency of the control mass p_3 and the pole location due to integral feedback p_0 were selected in accordance with various criteria depending upon the configuration.

CHAPTER IV

RESULTS

4.1 INTRODUCTION

As explained in the preceding chapter, the synthesis procedure employed in this study consists of (a) selecting (guessing) closed-loop, root locations, (b) calculating gains k_i which will yield these roots, and (c) obtaining the transient solutions to determine whether the force and deflection constraints have been violated. The trial-and-error character of this procedure is such that one is never quite sure that yet another try would not improve things. However, the solutions presented here are the result of a large number of such trial and error refinements. While some slight improvement might be achieved by additional effort, these results in general represent best-possible controller performance, i.e., optimum selection of gains k_i. Furthermore, the controller performance through a wide-range of configurations and operating conditions is consistently excellent.

The results presented in the following sections demonstrate the influence of the following factors on controller performance:

(a) stage of deployment,

(b) nominal spin velocity $\bar{\Omega}$, and

(c) torsional stiffness k_t.

The results consist of both tabular data and illustrations of transient solutions. The tabular data (which is presented for each case) contains the following information:

(a) ζ_i = ratio of effective to critical damping for all modes,

(b) p_1 = wobble frequency,

(c) p_2 = torsional natural frequency,

(d) specified closed-loop poles,

(e) calculated gains k_i,

(f) peak control force $|u|_{max}$, and

(g) peak control mass deflection $|w|_{max}$.

Transient solution illustrations are provided for the two fully-deployed configurations ($k_t = 0$, $k_t \neq 0$) both with and without control. In addition, transient solution illustrations are provided for the 1/2 deployed configuration ($k_t \neq 0$) at maximum spin velocity. These illustrations were included to provide a qualitative indication of the controller's effectiveness.

4.2 UNDEPLOYED SPACE STATION

The requisite input data for the undeployed space station is provided in the preceding chapter. As previously noted in Section 3.4, the nominal spin-velocity can equal or exceed 4 rpm. The two cases considered for the non-deployed configuration are (a) $\bar{\Omega}$ = 4 rpm and (b) $\bar{\Omega}$ = 11.5 rpm. An initial value of $\bar{\Omega}$ = 11.5 rpm. is sufficient to yield a spin-velocity of 4 rpm. for the fully-deployed configuration. The results for these two cases are illustrated in Tables 4.2(a) and (b). Inspection of these tables reveals that the lower spin-velocity case is the more easily controlled in the sense that a higher control force is required.

TABLE 4.2(a): Undeployed Configuration, $\bar{\Omega}$ = 4 rpm.

Input Data: $\bar{\Omega}$ = .418 rad./sec., p_1 = .1004 rad./sec.

Control Data: ζ_1 = 1.0, ζ_3 = .1667

$k_1 = 1.815 \times 10^3$ lb.sec./rad., $k_2 = -3.767 \times 10^4$ lb.sec./rad.

k_5 = .1037 lb.sec./ft., k_6 = -4.456 lb./ft., k_7 = -.1109 lb./ft.sec.

Closed-Loop Pole Location

	Ω_x, Ω_y	w	$\int w$
real	-.1004	-.1004	-.0288
imag.	0.0	.5942	

Transient Performance:

$|u|_{max}$ = 15.9 lbs, $|w|_{max}$ = 16.2 ft.

TABLE 4.2(b): Undeployed Configuration, $\bar{\Omega}$ = 11.5 rpm.

Input Data: $\bar{\Omega}$ = 1.2035 rad./sec., p_1 = .2891 rad./sec.

Control Data: ζ_1 = 1.0, ζ_3 = .40

$k_1 = -1.081 \times 10^3$ lb.sec./rad., $k_2 = -1.626 \times 10^4$ lb.sec./rad.

k_5 = -10.91 lb.sec./ft., k_6 = -9.965 lb./ft., k_7 = -.1596 lb./ft.sec.

Closed-Loop Pole Location

	Ω_x, Ω_y	w	$\int w$
real	-.2892	-.2892	-.0288
imag	0.0	.6626	

Transient Performance

$|u|_{max}$ = 24.4 lbs., $|w|_{max}$ = 10.8 lbs.

4.3 CONTROL FOR $k_t = 0$.

a. The Fully Deployed Configuration $\bar{\Omega} = 4$ rpm

Since a space station will normally be in the fully deployed state the effectiveness of the MMC in providing attitude stabilization for this particular configuration is of fundamental interest. Evidence for the controller's superior performance is provided by a comparison of the uncontrolled motion illustrated in figure 3 with the controlled motion in figure 4. In addition, from Table 4.3(a), the peak force and deflection magnitudes are seen to be $|w|_{max} = 16.5$ ft., and $|u|_{max} = 14.2$ lbs. Note is made that the gains on $\dot{\theta}$ and θ (k_3 and k_4) are zero, and this is characteristic of all $k_t = 0$ cases. Since no disturbance torque is applied to the crew quarters due to θ motion, there is no reason to attempt control of the relative torsional motion.

TABLE 4.3(a). The Fully Deployed Configuration, $\bar{\Omega} = 4$ rpm., $k_t = 0$.

Input Data: $p_1/\bar{\Omega} = .230$, $p_2/\bar{\Omega} = .223$

Control Data: $\zeta_1 = 1.0$, $\zeta_2 = 0.$, $\zeta_3 = .20$

$k_1 = 610.1$ lb.sec./rad., $k_2 = -1.561 \times 10^4$ lb.sec./rad., $k_3 = k_4 = 0.$,

$k_5 = -.634$ lb.sec./ft., $k_6 = -3.974$ lb./ft., $k_7 = -.0910$ lb./ft.sec.

Closed-Loop Pole Location

	Ω_x, Ω_y	w	θ	$\int w$
real	-.1109	-.1109	0.	-.0287
imag	.0093	.5431	.0933	

Transient Performance:

$|u|_{max} = 14.2$ lb., $|w|_{max} = 16.5$ ft.

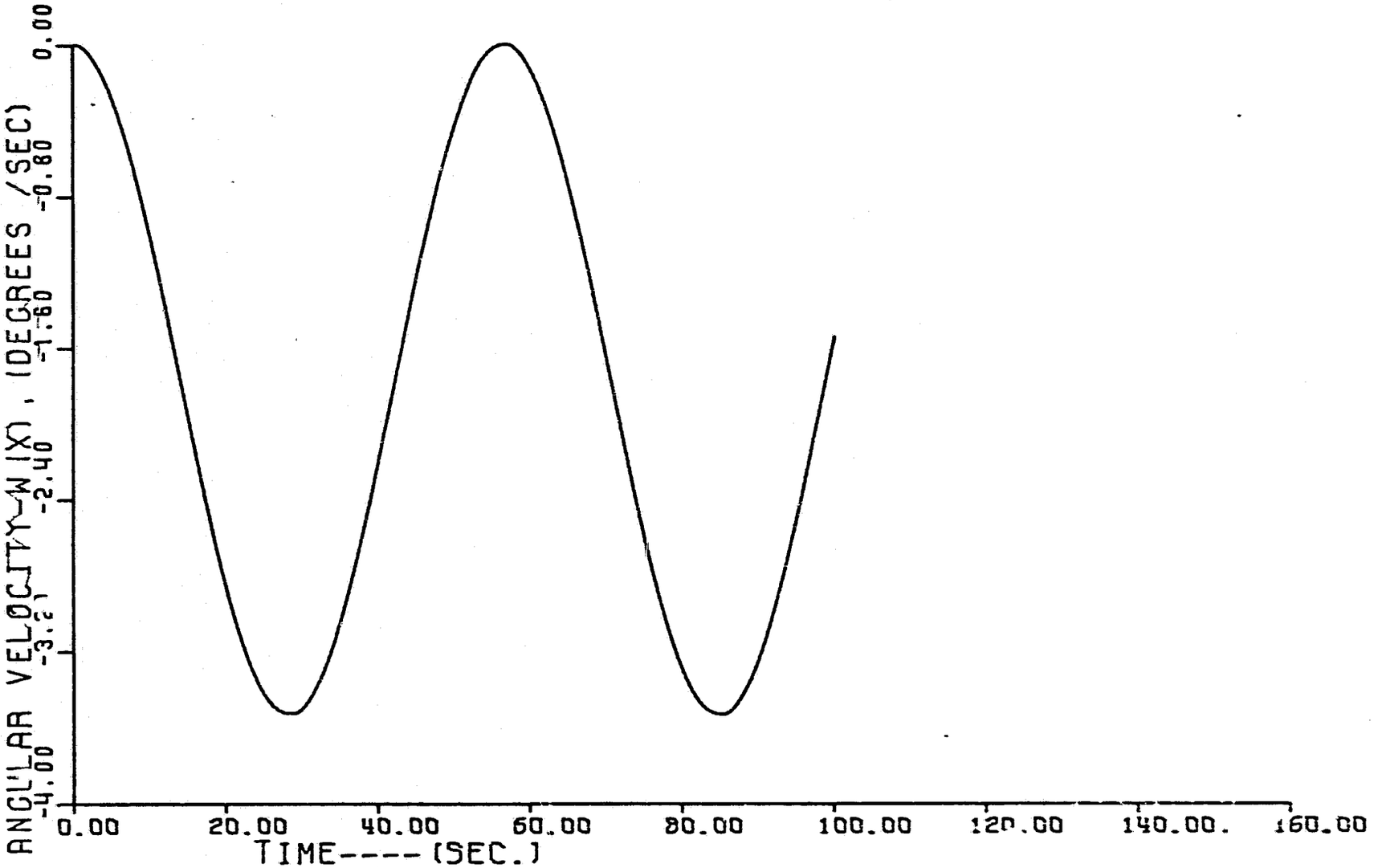

3.a Uncontrolled Motion: Ω_x versus t for the fully deployed configuration with $k_t = 0$, and $\overline{\Omega} = 4$ rpm

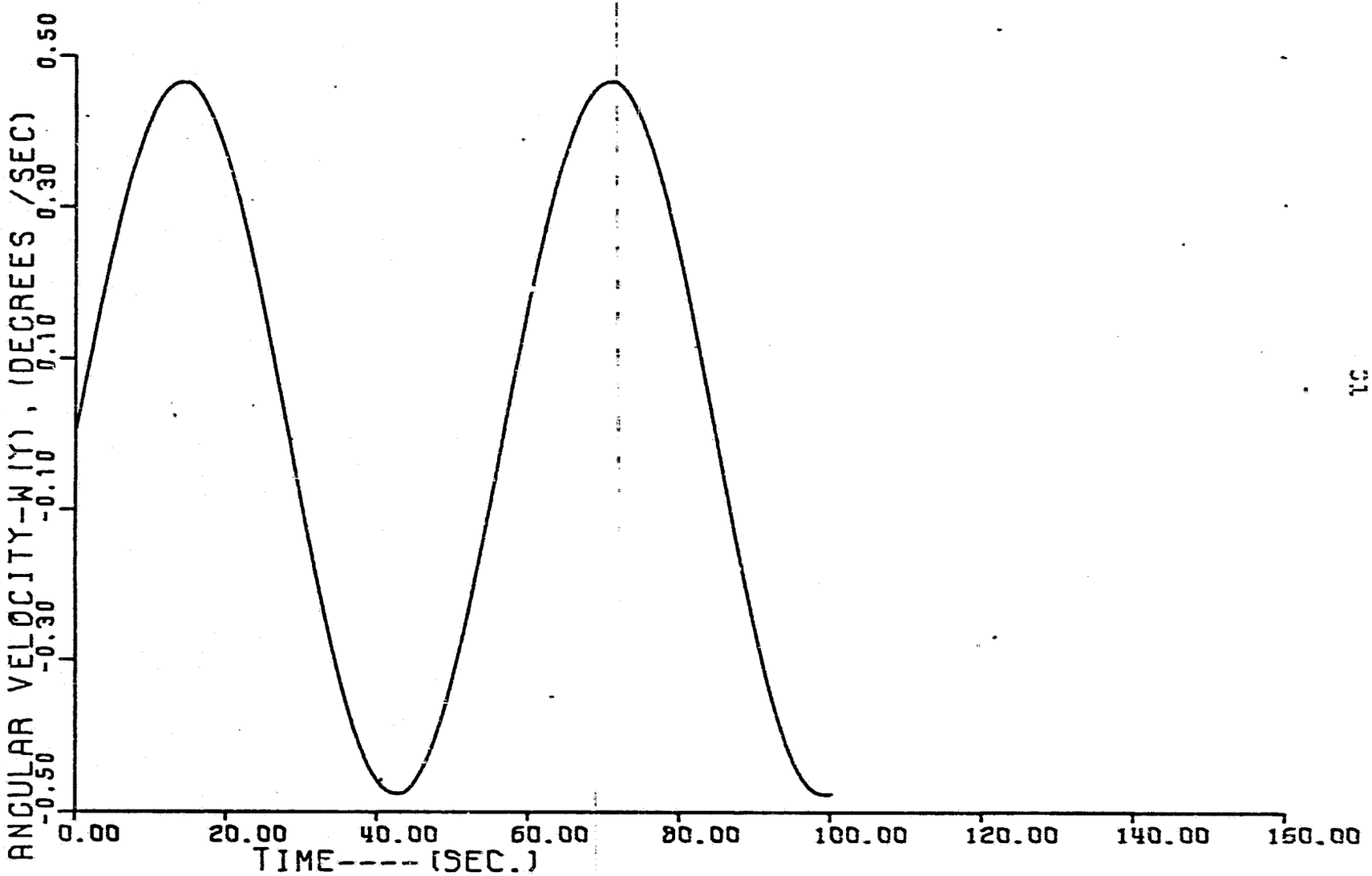

3.b Uncontrolled Motion: Ω_y versus t for the fully deployed configuration with $k_t = 0$, and $\bar{\Omega} = 4$ rpm.

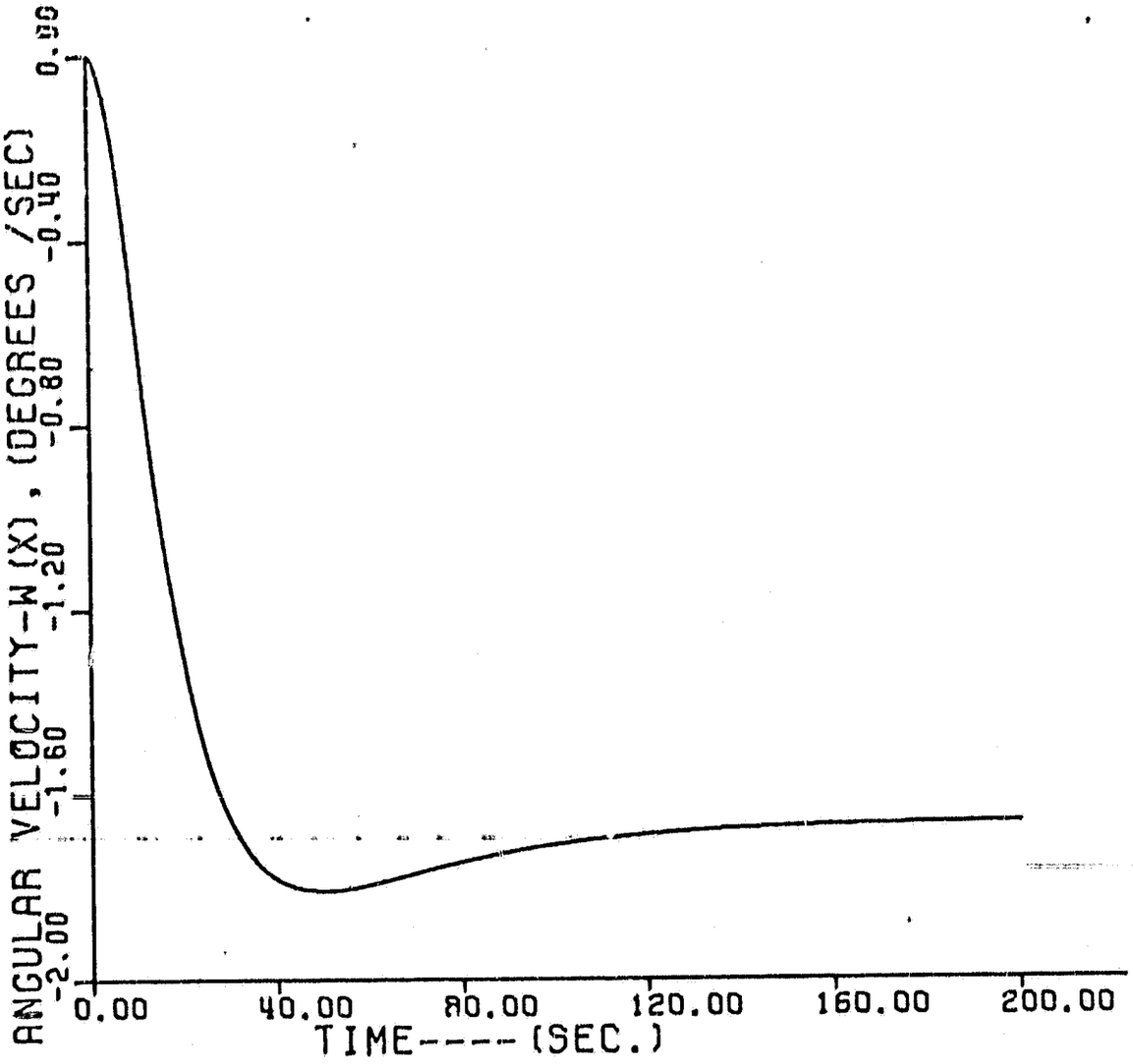

4.a Controlled Motion: Ω_x versus t for the fully deployed configuration with $k_t = 0$, and $\bar{\Omega}$=4rpm.

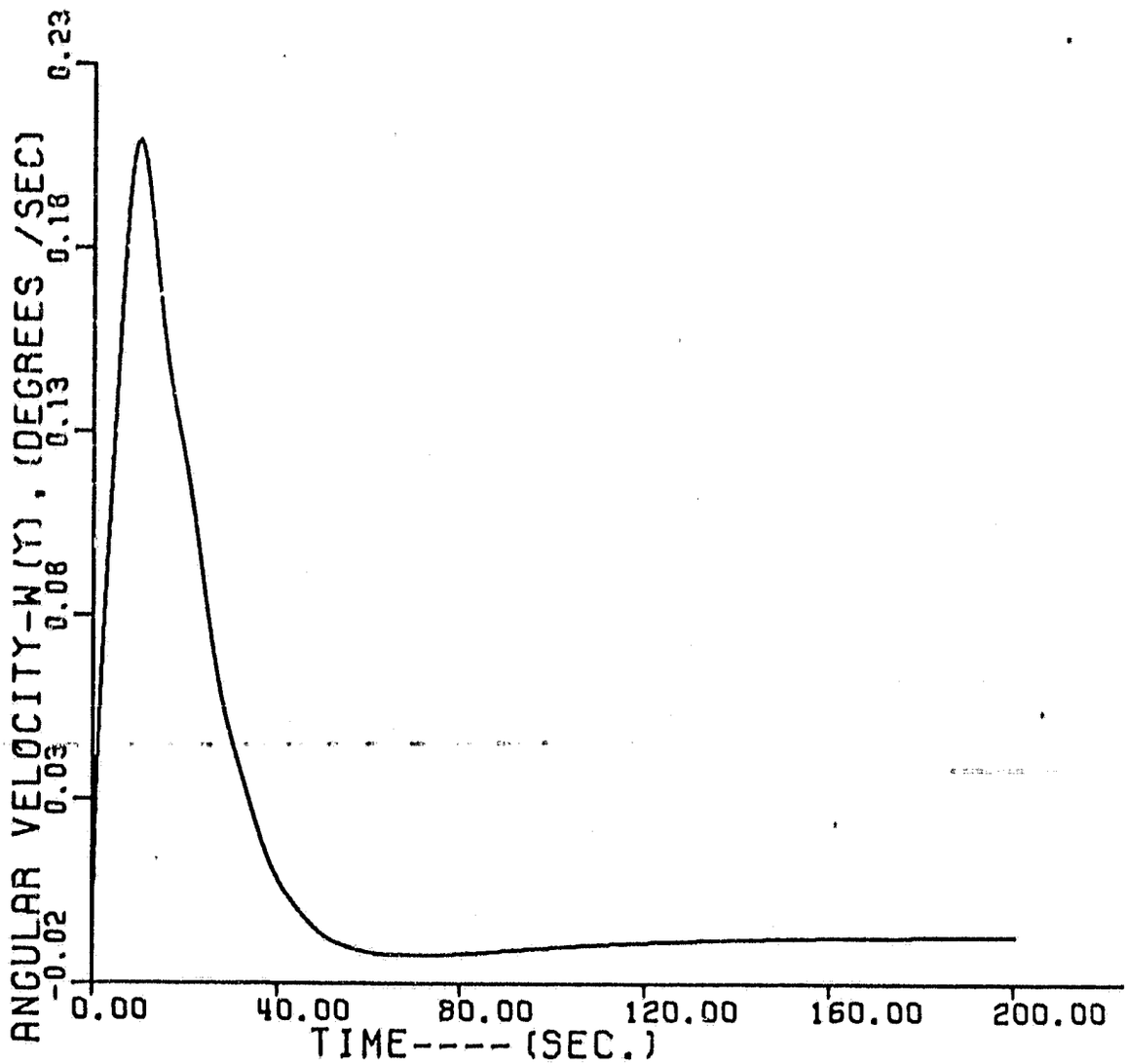

4.b Controlled Motion: Ω_y versus t for the fully deployed configuration with $k_t = 0$, and $\bar{\Omega} = 4$ rpm.

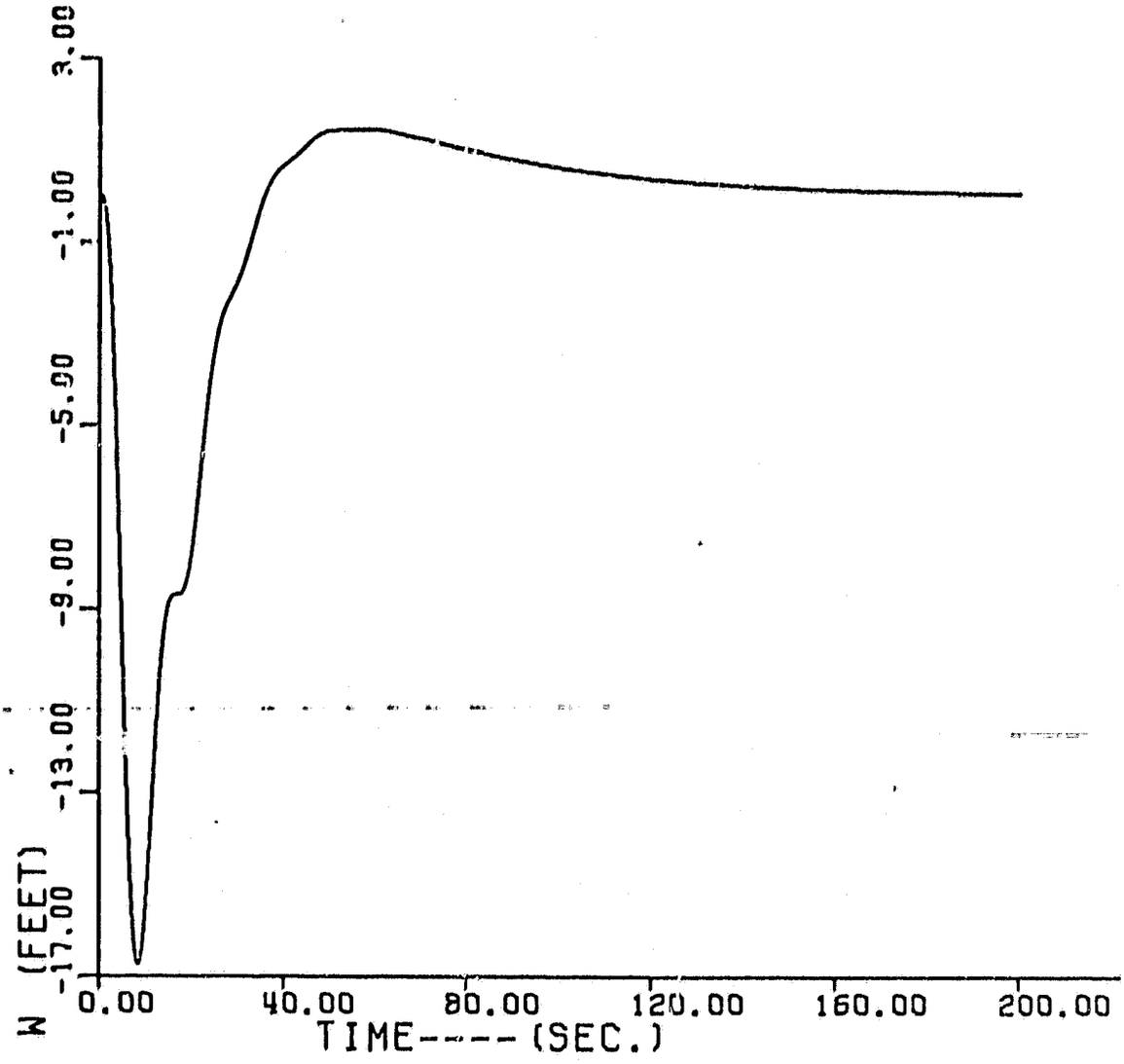

4.c Controlled Motion: w versus t for the fully deployed configuration with $k_t = 0$, and $\bar{\Omega}$ = 4rpm.

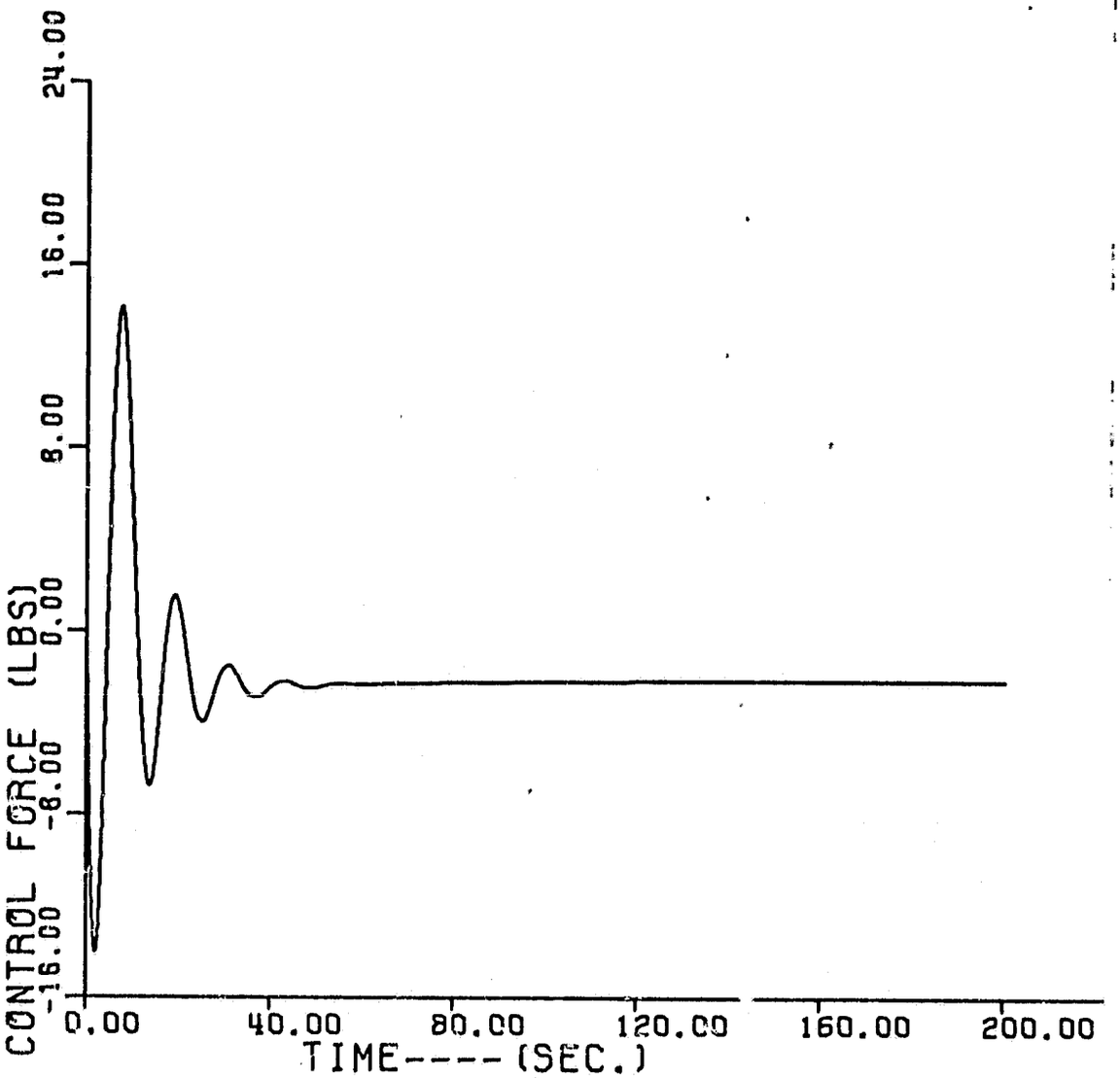

4.d Controlled Motion: u versus t for the fully deployed configuration with $k_t = 0$, and $\bar{\Omega} = 4$ rpm.

b. 3/4 Deployed Configuration, $\bar{\Omega}$ = 4 and 4.85 rpm

The results for this case are summarized in Table 4.3(b). A comparison of these results with those on Table 4.3(a) reveals scant differences between the 3/4 and the fully deployed configuration when $\bar{\Omega}$ = 4 rpm. This comparative insensitivity to the state of deployment can be explained by noting that the only factors which vary in the governing Eq.(26) due to deployment are a, r_y/I_x, and $e = I^2_y/I_x$. The latter two parameters are small, and have a comparatively minor influence on the systems' behavior. Conversely, the dependency of the wobble frequency p_1 upon a (Eq. (25)) makes it a significant parameter. However, Table B reveals that a only changes slightly from the non-deployed to the fully deployed configuration.

A comparison of the results of case 1 and 2 in Table 4.3(b) demonstrates the marked dependence of controller performance upon the nominal spin velocity. The natural frequencies p_1, p_2 display the predicted (Eq. (25)) linear dependence upon $\bar{\Omega}$ while the peak force $|u|_{max}$ increases markedly with increasing $\bar{\Omega}$.

c. 1/2 Deployed Configuration, $\bar{\Omega}$ = 4 and 6.23 rpm.

The results for these two cases are presented in Table 4.3(c), and continue to demonstrate (a) the comparative insensitivity to the stage of deployment, and (b) the marked dependence of controller performance upon the nominal spin velocity $\bar{\Omega}$.

d. 1/4 Deployed Configuration, $\bar{\Omega}$ = 4 and 8.3 rpm

The results for these two cases are presented in Table 4.3(d), and represent basically the same controller behavior cited previously for the 1/2 deployed configuration.

TABLE 4.3(b): 3/4 Deployed Configuration, $k_t = 0.0$

Case 1: $\bar{\Omega}$ = 4 rpm = .418 rad./sec.

Input Data: $p_1/\bar{\Omega} = .230$, $p_2/\bar{\Omega} = .223$

Control Data: $\zeta_1 = 1.0$, $\zeta_2 = 0.$, $\zeta_3 = .1667$

$k_1 = 1.023 \times 10^3$ lb.sec./rad., $k_2 = -2.259 \times 10^4$ lb.sec./rad.

$k_3 = k_4 = 0$, $k_5 = 1.399$ lb.sec./ft., $k_6 = -5.3940$ lb./ft.

$k_7 = -1.309$ lb./ft.sec.

Closed-Loop Pole Location:

	Ω_x, Ω_y	w	θ	∫w
real	-.1109	-.1109	0.	-.0286
imag.	.0108	.6554	.0932	

Transient Performance:

$|u|_{max} = 19.1$ lb., $|w|_{max} = 16.5$ ft.

Case 2: $\bar{\Omega}$ = 4.85 rpm = .507 rad./sec.

Input Data: $p_1/\bar{\Omega} = .230$, $p_2/\bar{\Omega} = .223$

Control Data: $\zeta_1 = 1.0$, $\zeta_2 = 0.0$, $\zeta_3 = .1667$

$k_1 = 914.1$ lb.sec./rad., $k_2 = -2.729 \times 10^4$ lb.sec./rad.

$k_3 = k_4 = 0$, $k_5 = 1.732$ lb.sec./ft., $k_6 = -7.947$ lb./ft..

$k_7 = -.19257$ lb./ft.sec.

Closed-Loop Pole Location:

	Ω_x, Ω_y	w	θ	∫w
real	-.1344	-.1344	0.	-.0286
imag.	.0125	.7950	.1131	

Transient Performance:

$|u|_{max} = 28.0$ lbs., $|w|_{max} = 16.5$ ft.

TABLE 4.3(c): 1/2 Deployed Configuration, $k_t = 0.0$

Case 1: $\bar{\Omega}$ = 4 rpm = .418 rad./sec.

Input Data: $p_1/\bar{\Omega} = .230$, $p_2/\bar{\Omega} = .223$

Control Data: $\zeta_1 = 1.0$, $\zeta_2 = 0.0$, $\zeta_3 = .250$

$k_1 = 268.26$ lb.sec./rad., $k_2 = -9.785 \times 10^3$ lb.sec./rad.

$k_3 = k_4 = 0$, $k_5 = -2.3147$ lb.sec./ft., $k_6 = -2.794$ lb./ft.

$k_7 = -.0580$ lb./ft.sec.

Closed-Loop Pole Location:

	Ω_x, Ω_y	w	θ	$\int w$
real	-.1107	-.1107	0.0	-.0286
imag.	.0117	.4285	.0932	

Transient Performance:

$|u|_{max} = 9.7$ lb. , $|w|_{max} = 16.1$ ft.

Case 2: $\bar{\Omega}$ = 6.23 rpm = .652 rad./sec.

Input Data: $p_1/\bar{\Omega} = .243$, $p_2/\bar{\Omega} = .223$

Control Data: $\zeta_1 = 1.0$, $\zeta_2 = 0.0$, $\zeta_3 = .20$

$k_1 = 358.6$ lb.sec./rad., $k_2 = -2.393 \times 10^4$ lb.sec./rad.

$k_3 = k_4 = 0.$, $k_5 = -.9139$ lb.sec./ft.

$k_6 = -9.619$ lb./ft., $k_7 = -.2206$ lb./ft.sec

Closed-Loop Pole Locations:

	Ω_x, Ω_y	w	θ	$\int w$
real	-.1726	-.1726	0.0	-.0287
imag.	.0170	.8455	.1453	

Transient Performance:

$|u|_{max} = 34.0$ lbs., $|w|_{max} = 16.5$ ft.

TABLE 4.3(d): 1/4 Deployed Configuration, $k_t = 0.0$

Case 1: $\bar{\Omega}$ = 4 rpm = .418 rad./sec.

Input Data: $p_1/\bar{\Omega} = .230$, $p_2/\bar{\Omega} = .223$

Control Data: $\zeta_1 = 1.0$, $\zeta_2 = 0.0$, $\zeta_3 = .1667$

$k_1 = 1.013 \times 10^4$ lb.sec./rad., $k_2 = -2.238 \times 10^4$ lb.sec./rad.

$k_3 = k_4 = 0$, $k_5 = 1.350$ lb.sec./ft., $k_6 = 5.362$ lb./ft.

$k_7 = -.1301$ lb./ft.sec.

Closed-Loop Pole Locations:

	Ω_x, Ω_y	w	θ	∫w
real	-.1105	-.1105	0.0	-.0285
imag.	.0140	.65342	.0931	

Transient Performance

$|u|_{max} = 19.0$ lb., $|w|_{max} = 16.5$ ft.

Case 2: $\bar{\Omega}$ = 8.3 rpm = .867 rad./sec.

Input Data: $p_1/\bar{\Omega} = .254$, $p_2/\bar{\Omega} = .223$

Control Data: $\zeta_1 = 1.0$, $\zeta_2 = 0.$, $\zeta_3 = .333$

$k_1 = -357.9$ lb.sec./rad., $k_2 = -1.060$ lb.sec./rad.

$k_3 = k_4 = 0.$, $k_5 = -7.258$ lb.sec./ft., $k_6 = -7.880$ lb./ft.

$k_7 = -.1400$ lb./ft.sec.

Closed-Loop Pole Location:

	Ω_x, Ω_y	w	θ	∫w
real	-.2293	-.2289	0.0	-.0287
imag.	.0221	.6478	.1931	

Transient Performance:

$|u|_{max} = 23.9$ lb., $|w|_{max} = 12.9$ ft.

4.4 CONTROL FOR FINITE TORSIONAL STIFFNESS

a. The Fully Deployed Configuration, $\bar{\Omega}$ = 4 rpm

The obvious observation that a cable-connected space station will be fully-deployed throughout most of its lifetime makes establishment of effective control for this particular stage of fundamental importance. Evidence for the controllers' superior performance is provided by a comparison of the uncontrolled motion illustrated in figure 5 with the controlled motion illustrated in figure 6. From table 4.4(a), the controlled motion of figure 5 corresponds to critical wobble damping rates, and results in the peak force magnitude $|u|_{max}$ = 16.1 lb., and peak deflection magnitude $|w|_{max}$ = 16.3 ft.

TABLE 4.4(a): The Fully Deployed Configuration, $\bar{\Omega}$ = 4 rpm

Input Data: $k_t = 1.463 \times 10^5$ ft.lb./rad.

$p_1/\bar{\Omega} = .230$, $p_2/\bar{\Omega} = 1.36$

Control Data: $\zeta_1 = 1.$, $\zeta_2 = .169$, $\zeta_3 = .167$

$k_1 = 3061.$ lb.sec./rad., $k_2 = -5.063 \times 10^4$ lb.sec./rad.,

$k_3 = -3.052 \times 10^4$ lb.sec./rad., $k_4 = 2.215 \times 10^3$ lb./rad.

$k_5 = -1.764$ lb.sec./ft., $k_6 = -5.653$ lb./ft., $k_7 = -.161$ lb./ft.sec.

Closed-Loop Pole Location:

	Ω_x, Ω_y	w	θ	∫w
real	-.1109	-.1109	-.1109	-.0288
imag.	0.0	.6464	-.6559	

Transient Performance:

$|u|_{max}$ = 16.1 lb., $|w|_{max}$ = 16.3 ft.

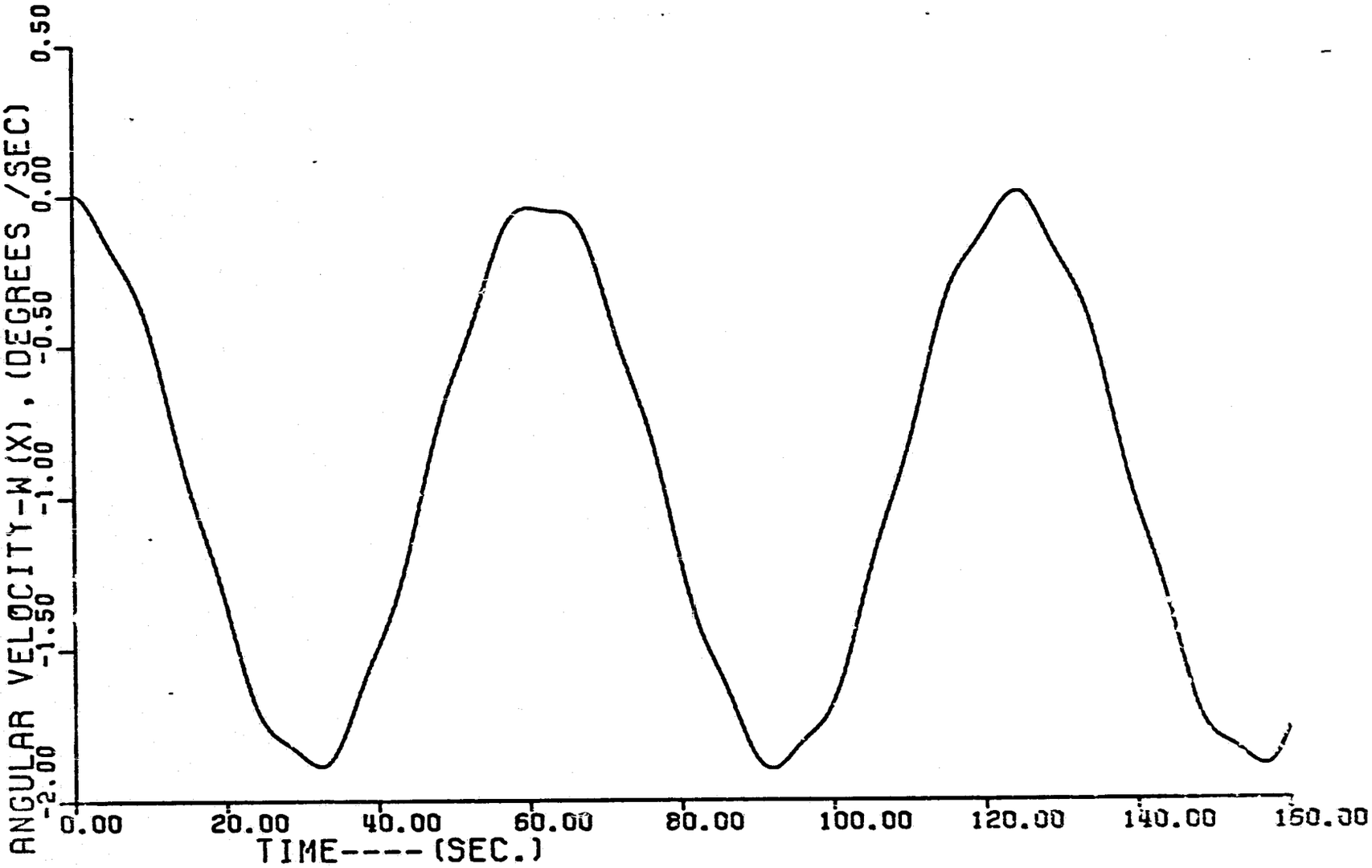

5.a Uncontrolled Motion: Ω_x versus t for the fully deployed configuration with $k_t = 1.463 \times 10^5$ ft.lbs/rad., and $\overline{\Omega}$ = 4rpm.

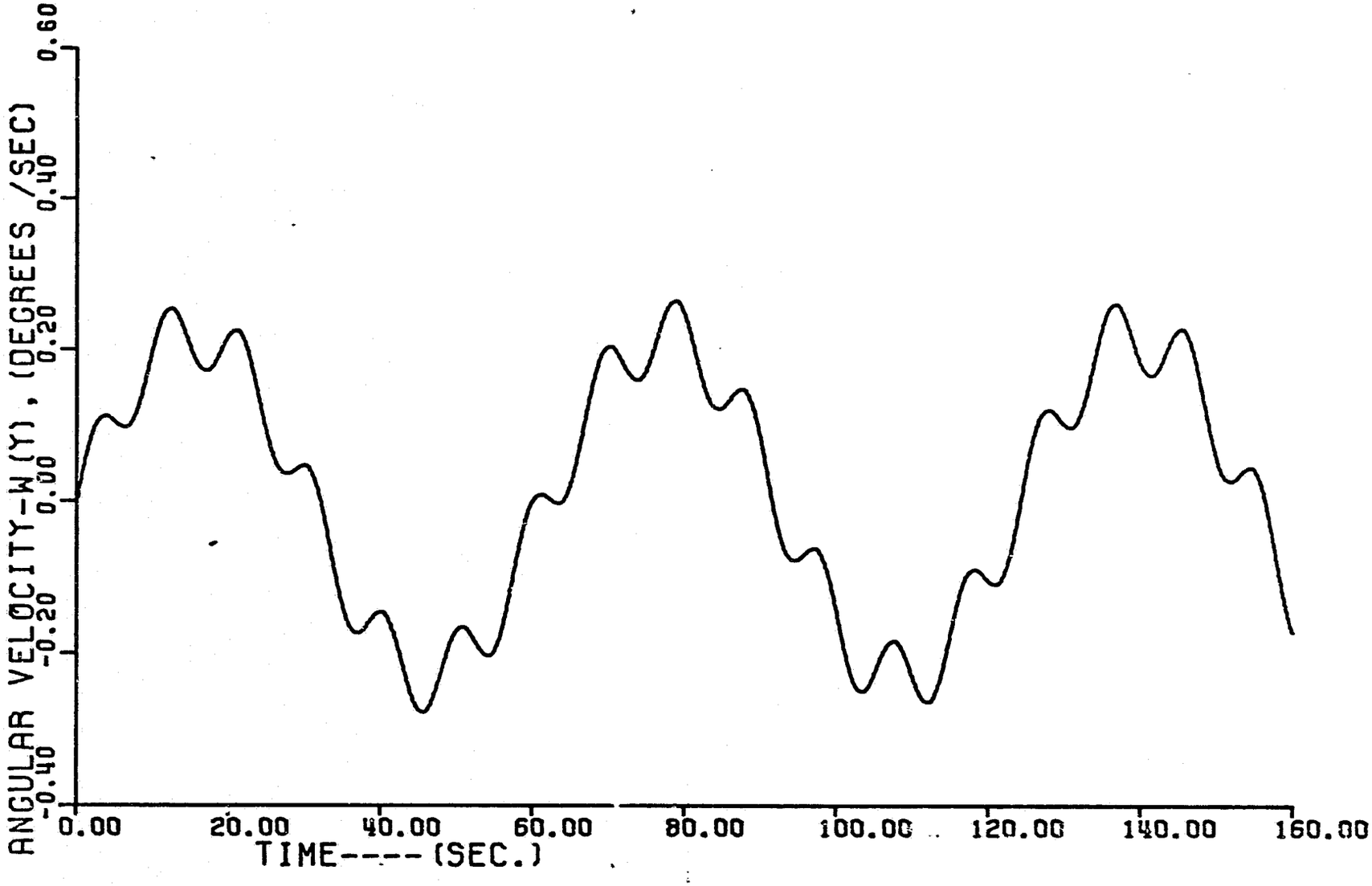

5.b Uncontrolled Motion: Ω_y versus t for the fully deployed configuration with k_t = 1.463 x10^{5}ft.lbs/rad., and $\bar{\Omega}$ = 4 rpm

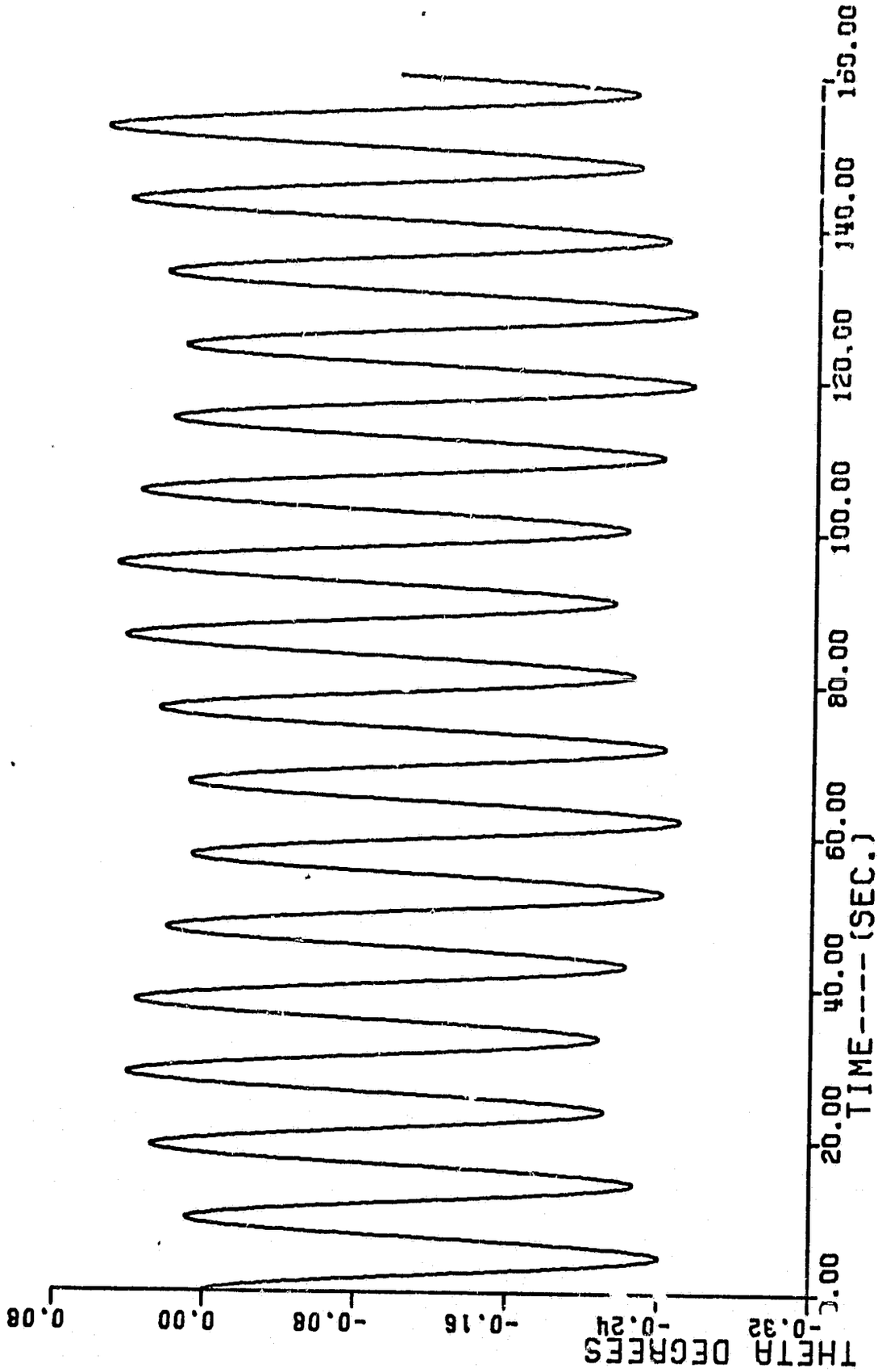

5.c Uncontrolled Motion: θ versus t for the fully deployed configuration with k_t = 1.463x 10^5 ft.lb./rad., and $\dot{\theta}$ =4rpm

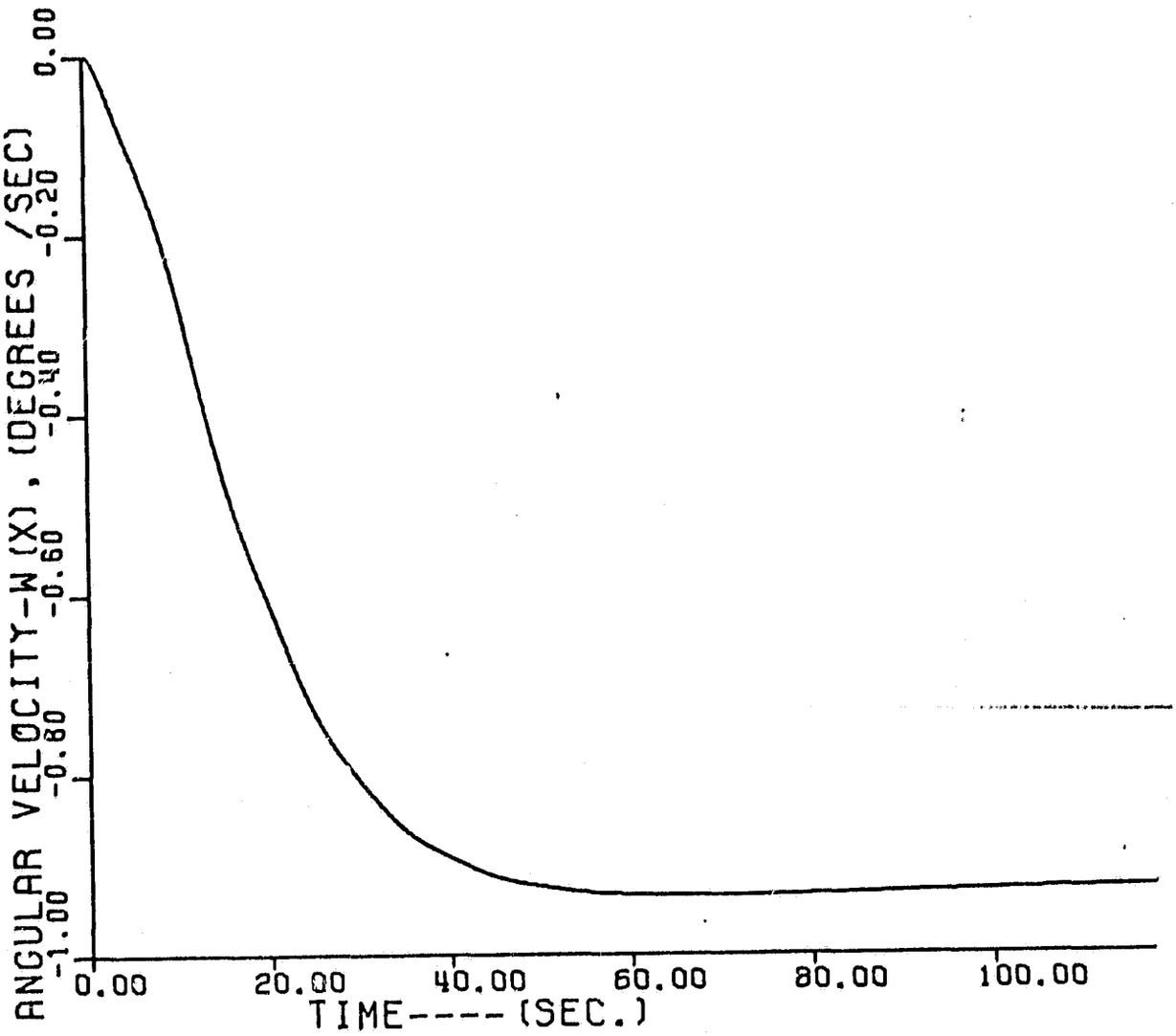

6.a Controlled Motion: Ω_x versus t for the fully deployed configuration with $k_t = 1.463 \times 10^5$ ft.lb./rad., and $\bar{\Omega} = 4$ rpm.

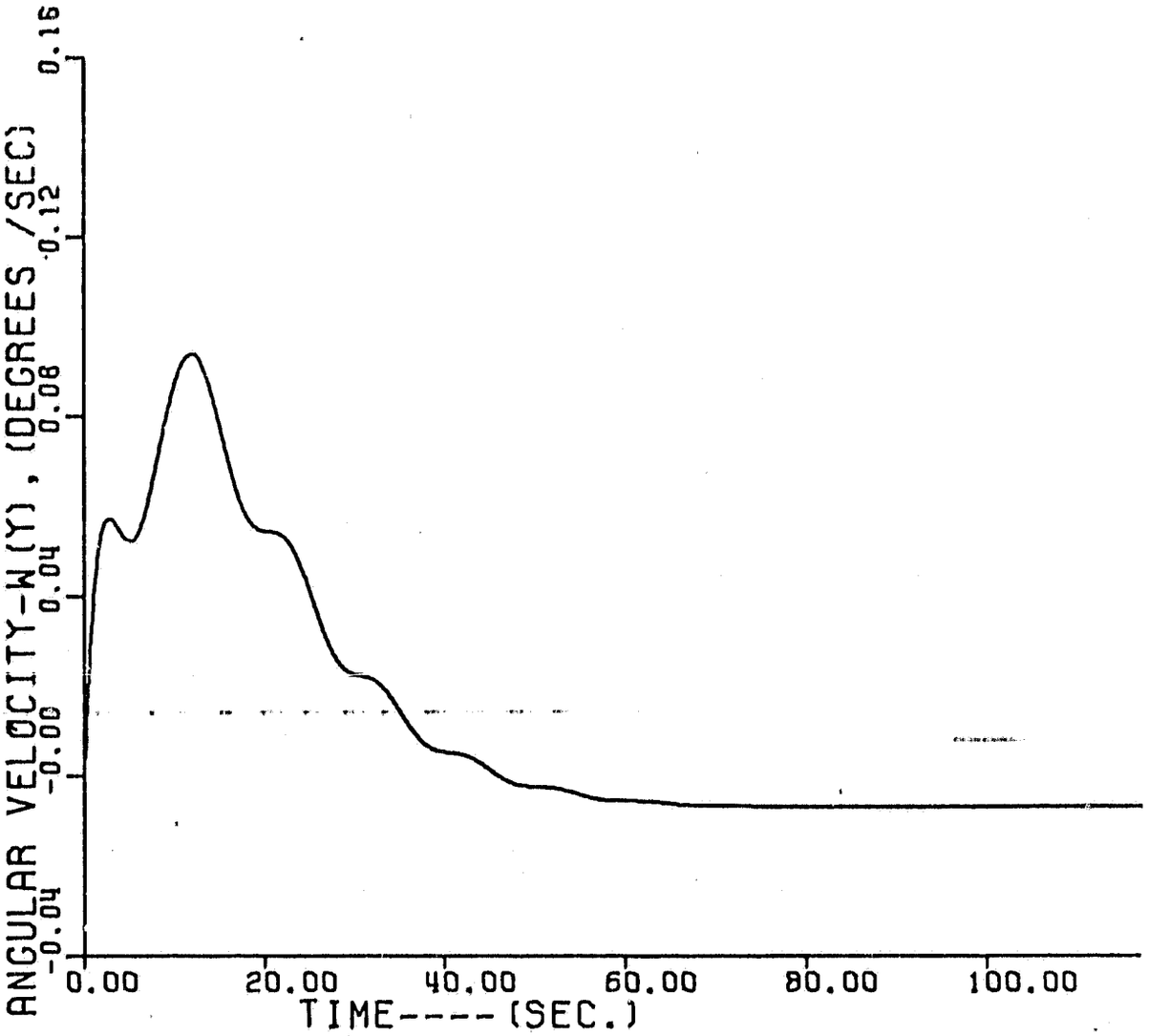

6.b Controlled Motion: Ω_y versus t for the fully deployed configuration with $k_t = 1.463 \times 10^5$ ft.lb./rad., and $\bar{\Omega} = 4$ rpm.

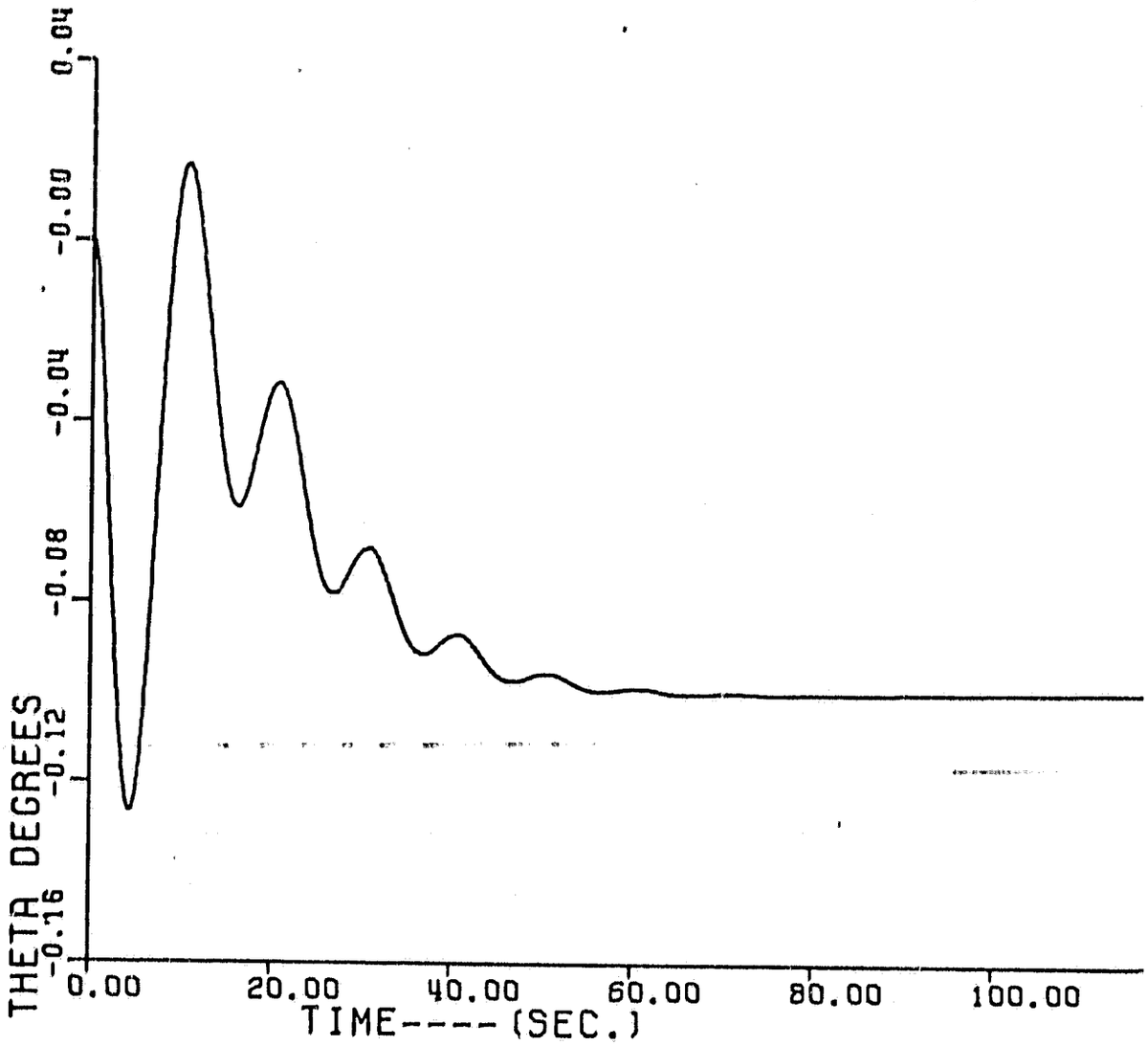

6.c Controlled Motion: θ versus t for the fully deployed configuration with $k_t = 1.463 \times 10^5$ ft.lb./rad., and $\bar{\Omega} = 4$ rpm.

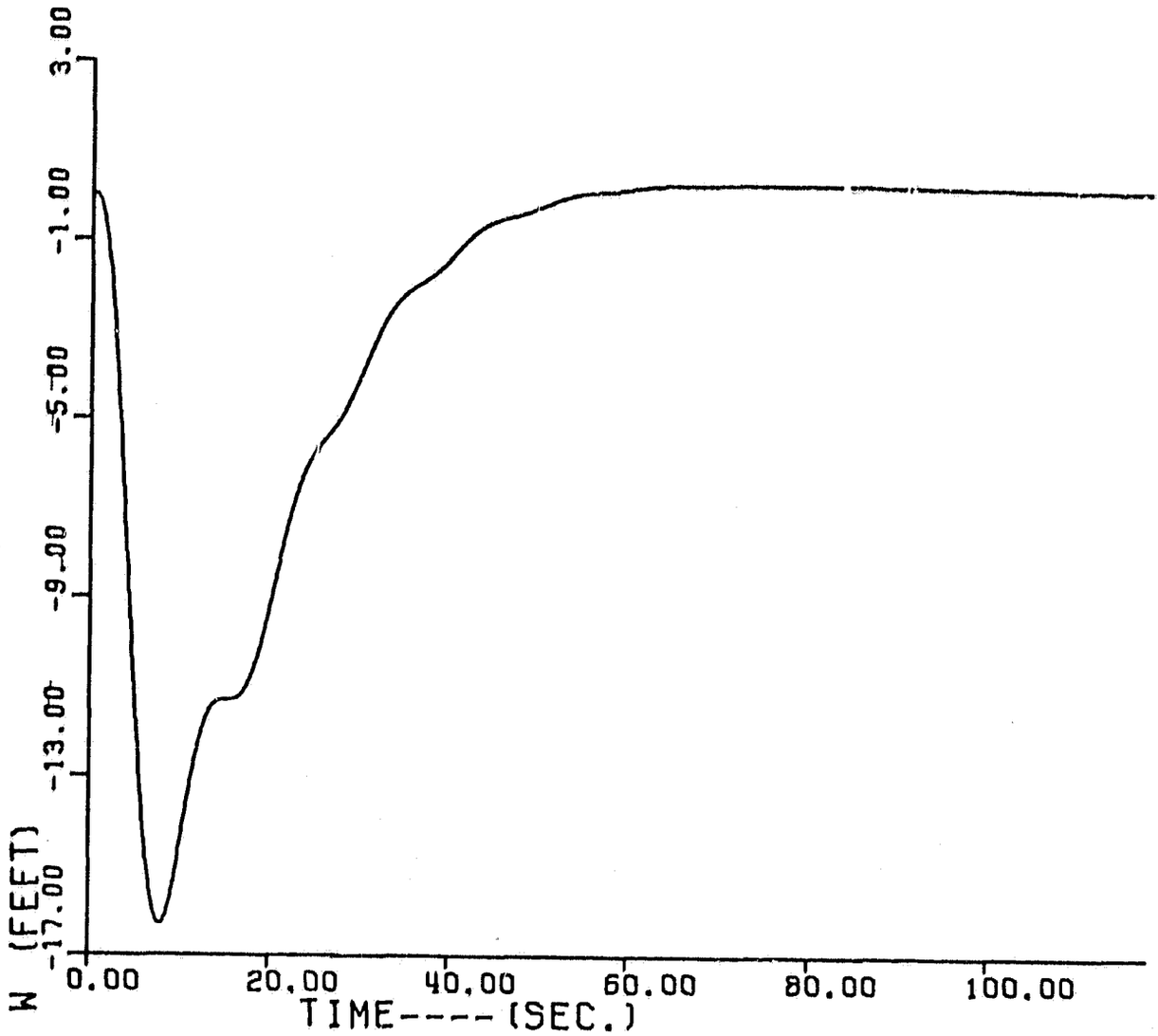

6.d Controlled Motion: w versus t for the fully deployed configuration with $k_t = 1.463 \times 10^5$ ft.lb./rad., and $\bar{\Omega} = 4$ rpm.

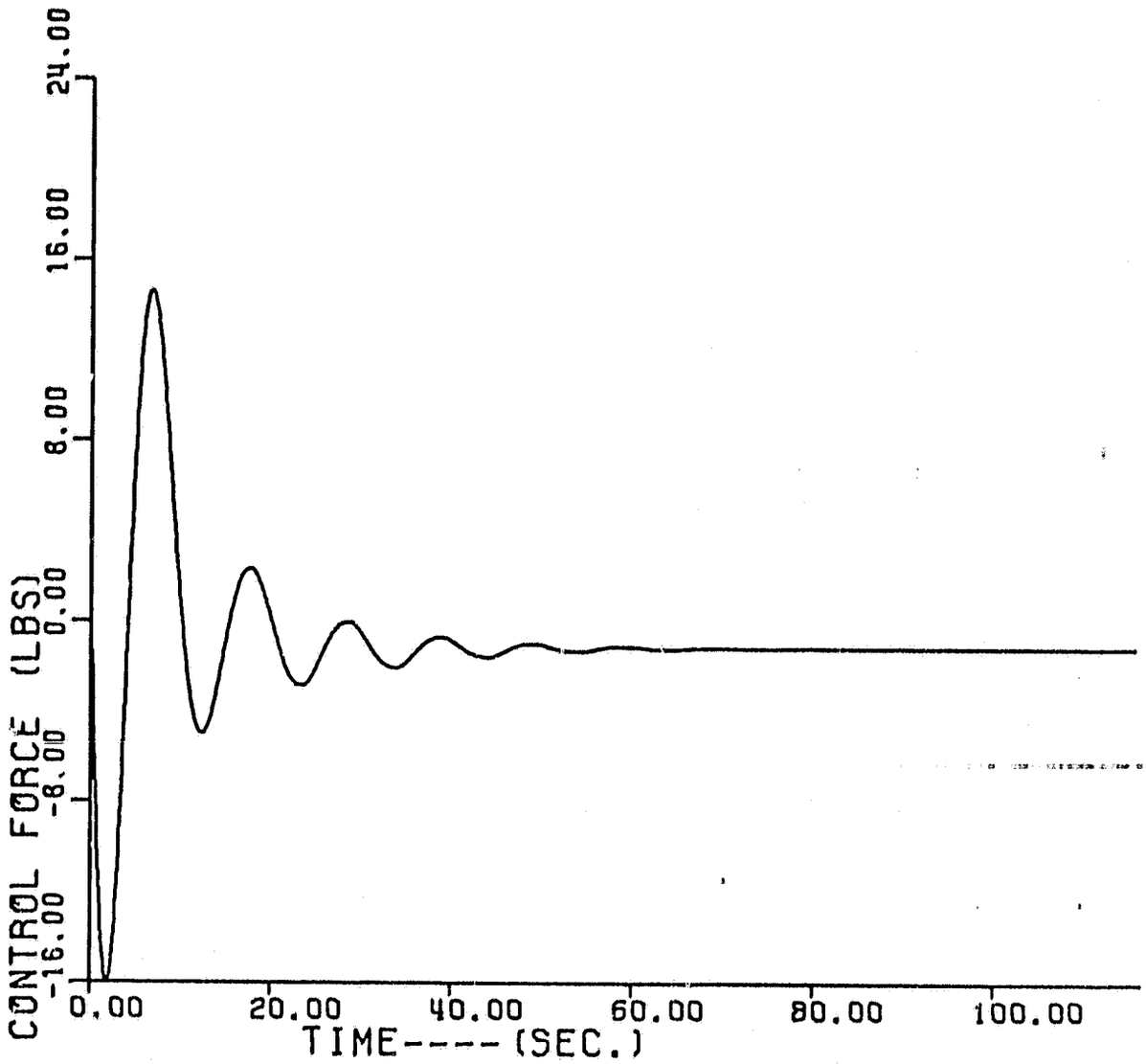

6.e Controlled Motion: u versus t for the fully deployed configuration with $k_t = 1.463 \times 10^5$ ft.lb./rad., and $\bar{\Omega} = 4$ rpm.

b. 3/4 Deployed Configuration, $\bar{\Omega}$ = 4 and 4.85 rpm.

The results for this case are summarized in Table 4.4(b). A comparison of these results withe those of 4.4(a) for $\bar{\Omega}$ = 4 rpm reveals that the only significant difference caused by a 3/4 retraction is an increase in k_t with a consequent increase in the torsional natural frequency p_2. However, in behavior which is very similar to that noted in the preceding section for $k_t = 0$, increasing $\bar{\Omega}$ causes an even more marked increase in k_t, p_1, and p_2. This result can be explained by noting that k_t is an (approximately) linear function of the tensile force in the cable, which is in turn proportional to $\bar{\Omega}^2$. These comparatively large values of k_t also couple wobble and torsional motion. Evidence of this coupling is demonstrated in figure 5 for uncontrolled space station motion.

c. 1/2 Deployed Configuration, $\bar{\Omega}$ = 4 and 6.23 rpm.

The results for these two cases are presented in Table 4.4(c), and continue to demonstrate (a) the comparative insensitivity to the stage of deployment, and (b) the marked dependence of controller performance upon the nominal spin-velocity $\bar{\Omega}$. The simulation results for the $\bar{\Omega}$ = 6.23 rpm case are presented in figures 7.a through 7.e. An inspection of these results confirms the effectiveness of the controller in providing initial wobble damping rates. The comparatively minor effect of the lightly damped (ζ_3 = .1364) torsional oscillations on wobble motion is evident in Figures 7.a and 7.b.

d. 1/4 Deployed $\bar{\Omega}$ = 4 and 8.3 rpm.

The results for these two cases are presented in Table 4.4(d), and reflect basically the same control cited above for the 1/2 deployed configuration.

F

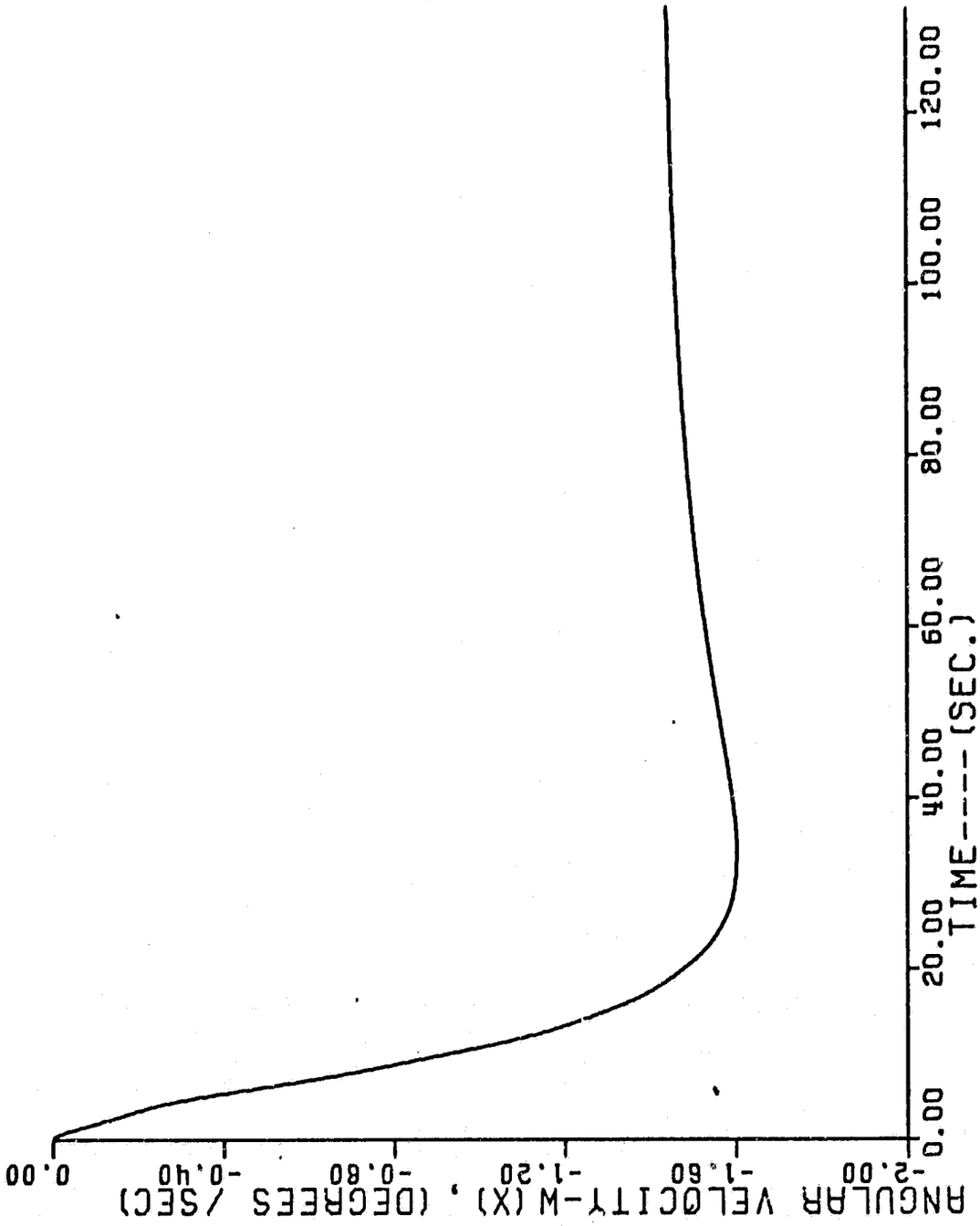

7.a Controlled Motion: Ω_x versus t for the 1/2 deployed configuration with $kt = 5.483 \times 10^5$ ft./rad., and $\bar{\Omega}$= 6.23 rpm.

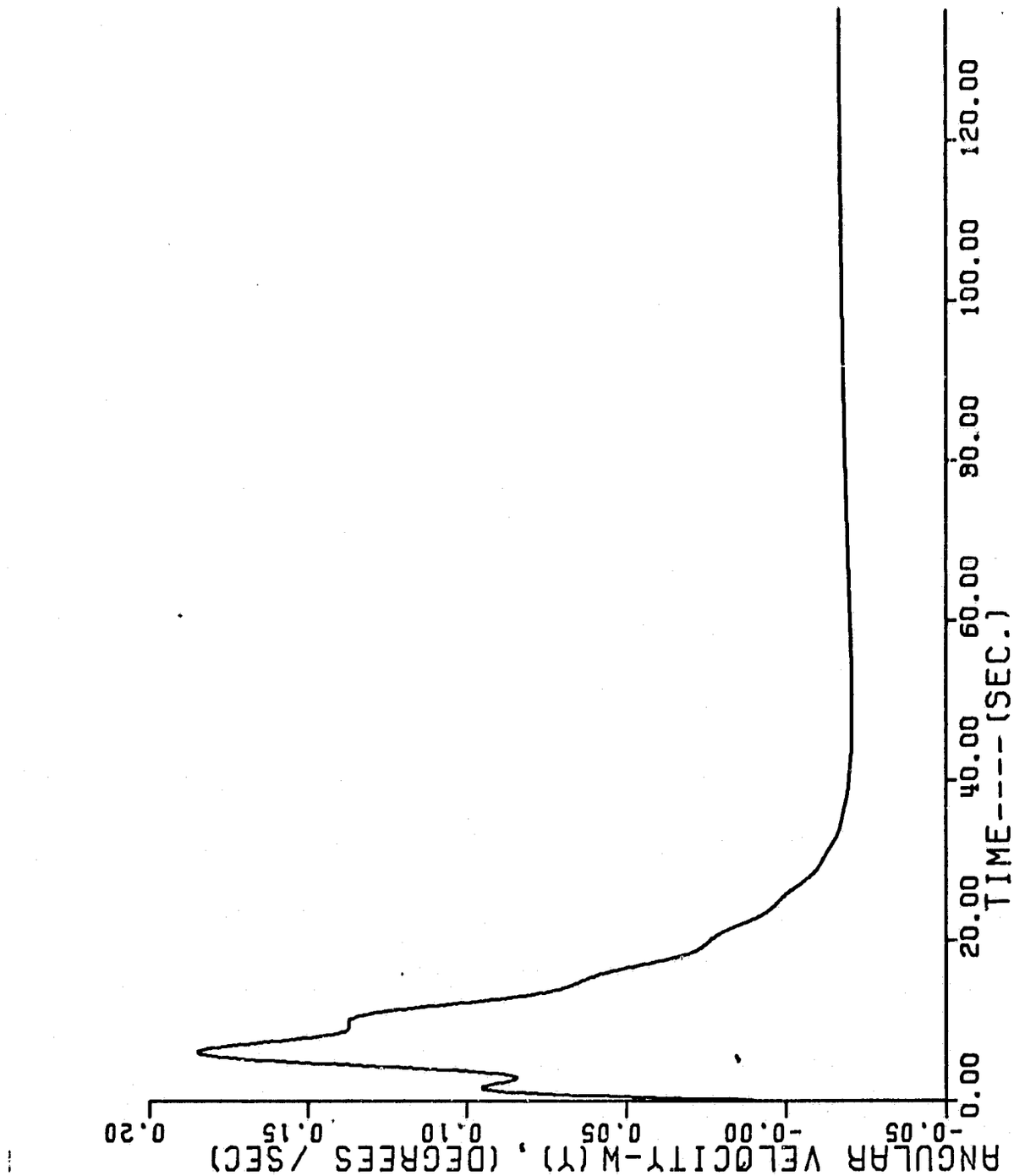

7.b Controlled Motion: Ω_y versus t for the 1/2 deployed configuration with $k_t = 5.483 \times 10^5$ ft.lb./rad., and $\bar{\Omega}$= 6.23 rpm.

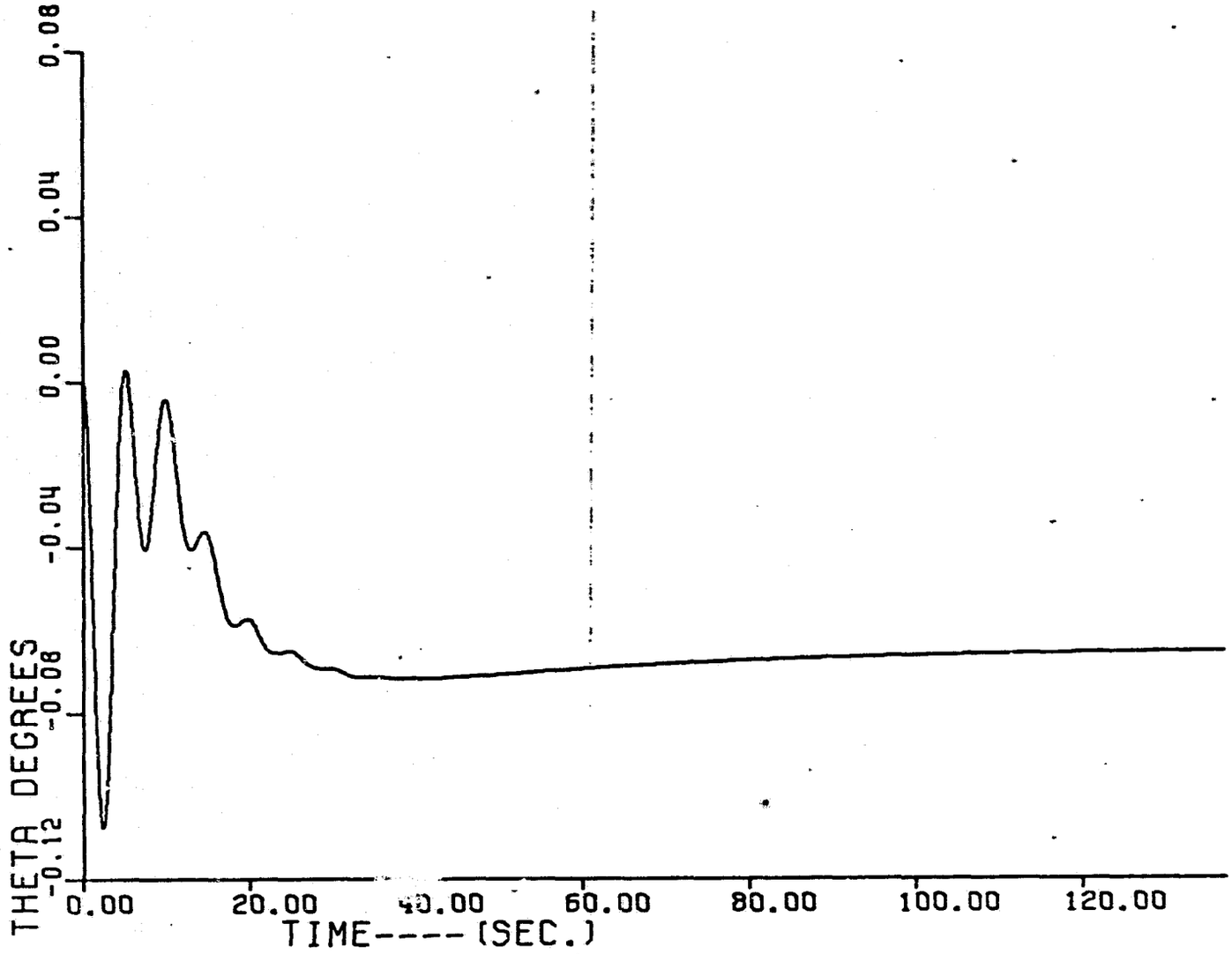

7.c Controlled Motion: θ versus t for the 1/2 deployed configuration with $k_t = 5.483 \times 10^5$ ft.lb./rad., and $\bar{\Omega} = 6.23$ rpm.

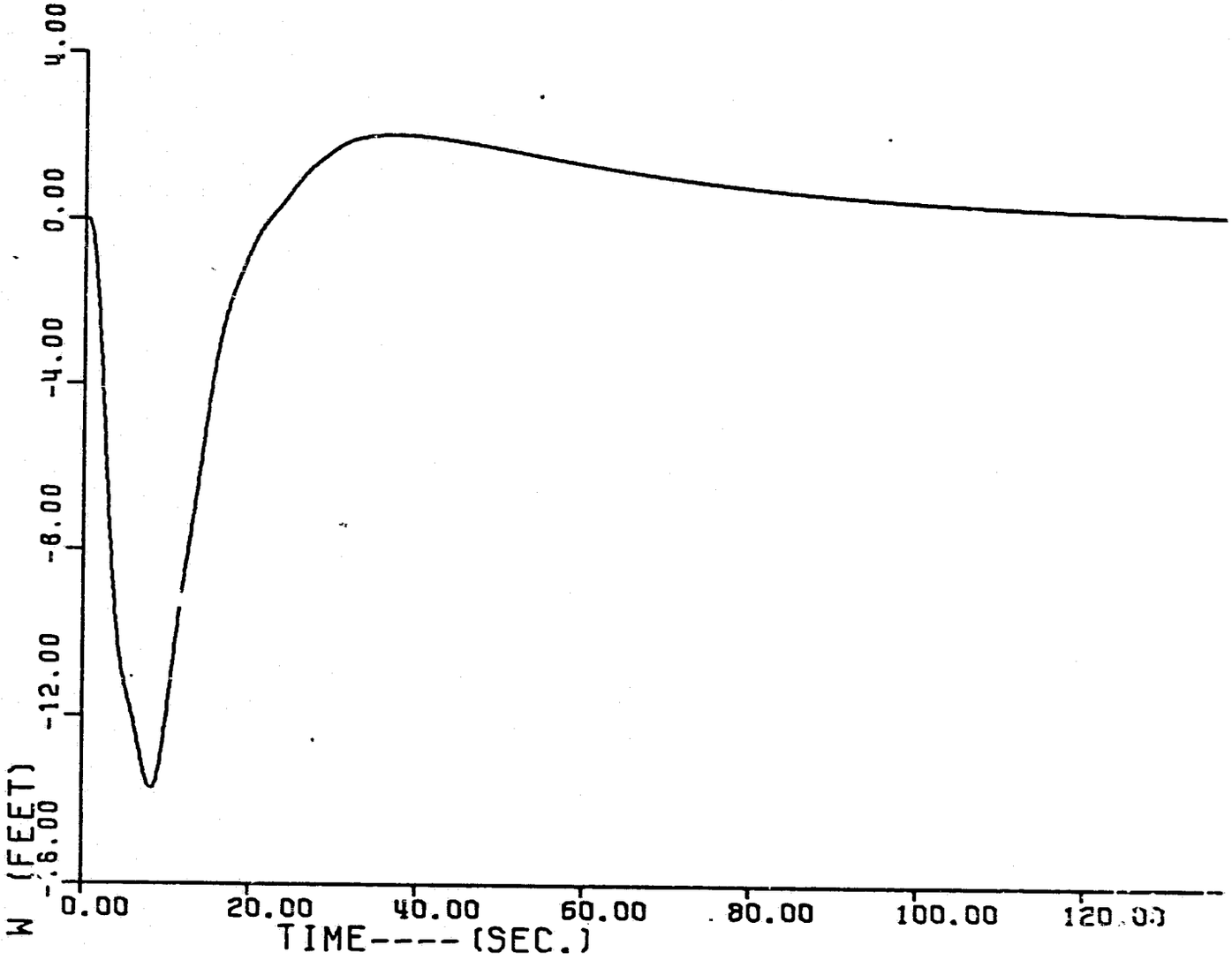

7.d Controlled Motion: w versus t for the 1/2 deployed configuration with k_t = 5.483 x 10^5 ft.lb./rad., and $\bar{\Omega}$ = 6.23 rpm.

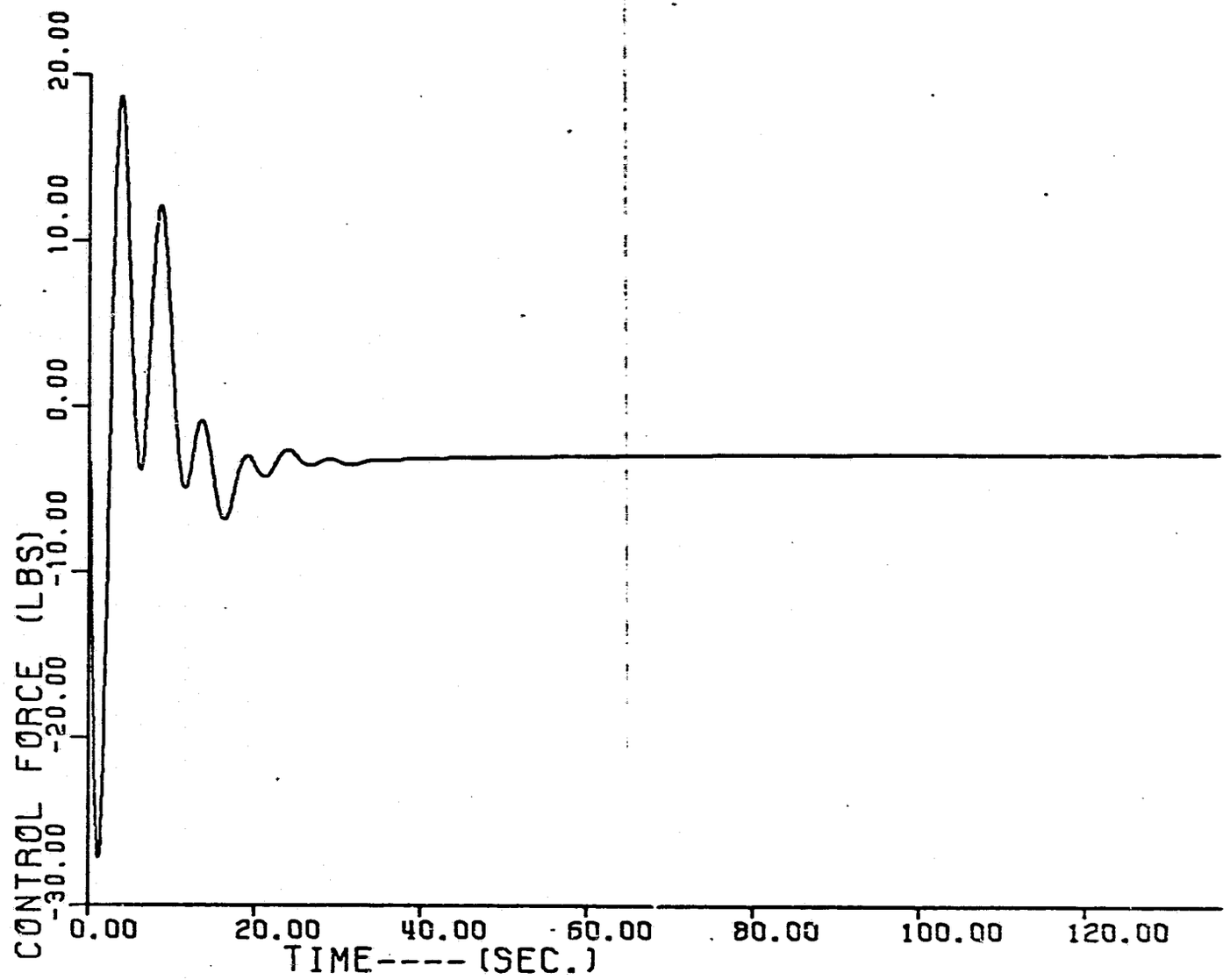

7.e Controlled Motion: u versus t for the 1/2 deployed configuration with k_t = 5.843 x 10^5 ft.lb./rad.,and $\overline{\Omega}$ = 6.23 rpm.

TABLE 4.4(b): 3/4 Deployed Configuration

Case 1: $\bar{\Omega}$ = 4 rpm. = .418 rad./sec., k_t = 1.726 x 10^5 ft.lb./rad.

Input Data: $p_1/\bar{\Omega}$ = .229, $p_2/\bar{\Omega}$ = 1.48

Control Data: ζ_1= 1.0 , ζ_2= .1557 , ζ_3= .2857

k_1 = 710.9 lb.sec./rad., k_2 = -1.694 x 10^4lb.sec./rad.

k_3 = -2.070 lb.sec./rad. , k_4 = 4.796 x 10^3lb./rad.

k_5 = -3.271 lb.sec./ft., k_6 = -1.993 lb./ft., k_7 = -.0547 lb./ft.sec.

Closed-Loop Pole Location:

	Ω_x, Ω_y	w	θ	∫w
real	-.1108	-.1108	-.1108	-.0288
imag.	0.0	.3716	.7027	

Transient Performance:

$|u|_{max}$ = 13.8 lb. , $|w|_{max}$ = 15.7 ft.

Case 2: $\bar{\Omega}$ = 4.85 rpm = .507 rad./sec., k_t' = 2.544 x 10^5ft.lb./rad.

Input Data: $p_1/\bar{\Omega}$ = .278 , $p_2/\bar{\Omega}$ = 1.79

Control Data: ζ_1= 1.0 , ζ_2= .1556 , ζ_3= .1667

k_1 = 3079. lb.sec./rad. , k_2 = -6.105 x 10^4lb.sec./rad.

k_3 = -3.385 lb.sec./rad., k_4 = 3.750 x 10^3lb./rad.

k_5 = -1.247 lb.sec./ft., k_6 = -8.198 lb./ft., k_7 = -.2367 lb./ft.sec.

Closed-Loop Pole Location

	Ω_x, Ω_y	w	θ	∫w
real	-.1344	-.1344	-.1344	-.0288
imag.	0.0	.8530	.7950	

Transient Performance:

$|u|_{max}$ = 25.4 lb., $|w|_{max}$ = 16.0 ft.

TABLE 4.4(c): 1/2 Deployed Configuration

Case 1: $\bar{\Omega}$ = 4 rpm. = .418 rad./sec., k_t = 2.254 x 10^5ft.lb./rad.

Input Data: $p_1/\bar{\Omega}$ = .229 , $p_2/\bar{\Omega}$ = 1.68

Control Data: ζ_1 = 1.0, ζ_2= .1364, ζ_3= .3333

k_1 = 373.8 lb.sec./rad., k_2 = -1.227 x 10^4lb.sec./rad.

k_3 = 1.491 x 10^3lb.sec./rad., k_4 = 4.691 x 10^3lb./rad.

k_5 = -3.578 lb.sec./ft., k_6 = -1.621 lb./ft.,k_7 = -.0402 lb./ft.sec

Closed-Loop Pole Location

	Ω_x, Ω_y	w	θ	∫w
real	-.1107	-.1107	-.1107	-.0288
imag.	0.0	.3130	.8036	

Transient Performance:

$|u|_{max}$ = 12.1 lbs. , $|w|_{max}$ = 14.9 ft.

Case 2: $\bar{\Omega}$ = 6.23 rpm = .652 rad./sec., k_t = 5.48 x 10^5ft.lb./rad.

Input Data: $p_1/\bar{\Omega}$ = .378 , $p_2/\bar{\Omega}$ = 2.77

Control Data: ζ_1= 1.0 , ζ_2= .1364, ζ_3= .40

k_1 = -174.96 lb.sec./rad., k_2 = -1.276 x 10^4lb.sec./rad.

k_3 = 6.907 x 10^3lb.sec./rad., k_4 = 1.181 x 10^4lb./rad.

k_5 -5.928 lb.sec /ft., k_6 = -2.893 lb./ft.,k_7 =-.0685 lb./ft.sec.

Closed-Loop Pole Location

	Ω_x, Ω_y	w	θ	∫w
real	-.1726	-.1726	-.1726	-.0288
imag.	0.0	.3955	1.254	

Transient Performance:

$|u|_{max}$ = 27.2 lb., $|w|_{max}$ = 13.7 ft.

TABLE 4.4(d): 1/4 Deployed Configuration

Case 1: $\bar{\Omega}$ = 4 rpm. = .418 rad./sec., k_t = 3.836 x 10^5 ft.lb./rad.

Input Data: $p_1/\bar{\Omega}$ = .228 , $p_2/\bar{\Omega}$ = 2.52

Control Data: ζ_1= 1.0, ζ_2= .1046, ζ_3= .20

k_1 = 2.156 x 10^3 lb.sec./rad., k_2 = -3.437 x 10^4 lb.sec./rad.

k_3 = -1.2608 x 10^4 lb.sec./rad., k_4 = 3.372 x 10^3 lb./rad.

k_5 = -1.255 lb.sec./ft., k_6 = -3.909 lb./ft., k_7= -.1113 lb./ft.sec.

Closed-Loop Pole Location:

	Ω_x, Ω_y	w	θ	∫w
real	-.1104	-.1104	-.1104	-.02878
imag.	0.0	.5411	1.050	

Transient Performance

$|u|_{max}$ = 15.8 lb., $|w|_{max}$ = 16.5 ft.

Case 2: $\bar{\Omega}$ = 8.3 rpm. = .867 rad./sec., k_t = 1.550 x 10^6 ft.lb./rad.

Input Data: $p_1/\bar{\Omega}$ = .254 , $p_2/\bar{\Omega}$ = 2.52

Control Data: ζ_1= 1.0, ζ_2= .1046 , ζ_3= 0.50

k_1 = -712.6 lb.sec./rad., k_2 = -1.010 x 10^4 lb.sec./rad.

k_3 = 1.782 x 10^4 lb.sec./rad., k_4 = 1.892 x 10^4 lb./rad.

k_5 = -8.685 lb.sec./ft., k_6 = -4.334 lb./ft., k_7 = -.0766 lb./ft.sec.

Closed-Loop Pole Location

	Ω_x, Ω_y	w	θ	∫w
real	-.2291	-.2291	-.2291	-.0288
imag.	0.0	.3968	2.177	

Transient Performance

$|u|_{max}$ = 34.9 lb., $|w|_{max}$ = 9.7 ft.

CHAPTER V

SUMMARY, CONCLUSIONS, AND EXTENSIONS

5.1 SUMMARY AND CONCLUSIONS

A dynamic model for cable-connected artificial-g space stations with an attached movable-mass-controller (MMC) system has been derived, and a linearized model for this system has been developed and its validity confirmed. This model has been used to examine the effectiveness of the MMC system in providing attitude stabilization for a space-station configuration reported by McDonnell-Douglas in Reference 8. The influence of the following three specific parameters were investigated:

(a) Stage of deployment. Undeployed, 1/4, 1/2, 3/4, and fully deployed stages were examined.

(b) Nominal spin-velocity $\bar{\Omega}$. This parameter was varied between 4 rpm and an upper value depending upon the stage of deployment.

(c) Torsional stiffness k_t. This parameter was varied from zero (corresponding to a single cable) to an upper value calculated for the McDonnell-Douglas design.

The MMC was required to provide critical wobble damping rates for all configurations without violating the peak-force-magnitude constraint, $|u| \leq 35$ lb., and the peak-deflection constraint, $|w| \leq 16.5$ ft. As discussed in Section 3.6, damping for the control mass and the torsional motion was provided to yield a uniform damping constant for wobble motion, control mass motion, and relative torsional motion, i.e.,

$$2\zeta_1 p_1 = 2\zeta_2 p_2 = 2\zeta_3 p_3$$

where the ζ_i are modal damping factors, and p_1, p_2, p_3 are the

"natural frequencies" associated with wobble, torsional, and control mass motion, respectively. In all cases ζ_1 was required to be unity (critical wobble damping); hence,

$$\zeta_2 = p_1/p_2 \ , \ \zeta_3 = p_1/p_3 \tag{37}$$

The natural frequency, p_3 was positioned arbitrarily (within reason) for each case by a proper selection of the feedback gains; however, the wobble frequency p_2 and torsional natural frequency p_2 are physical parameters which depend on the configuration, (i.e., spin velocity, asymmetry, torsional stiffness, etc.).

The procedure for comparing the controller's performance for the various cases is markedly simplified by the synthesis procedure employed, since the "quality" of control is the same for all cases. Specifically, for all cases, wobble motion is critically damped ($\zeta_1=1$), and all modal damping constants are equal. Hence, the significant point in a comparison of cases is the required maximum control force $|u|_{max}$ and control mass deflection $|w|_{max}$.

As previously noted, these two variables are of interest because of the physical constraint on $|w|$, and the prescribed constraint on $|u|$. They also indicate whether control torques arise primarily due to the control force u or control mass displacements w. Control torques directly caused by u are generated via the moment terms ur_x and ur_y, while torques due to w are generated via product of inertia terms $m_c r_x w\bar{\Omega}^2$ and $m_c r_y w\bar{\Omega}^2$. From a controls mechanization viewpoint, the variable $|u|_{max}$ should be minimized, while $|w|_{max}$ is maximized, i.e., $|w|_{max} = 16.5$ ft. In other words, one would like to employ a comparatively small and slowly-varying control force, and generate the required control torques primarily

through the "leisurely" manipulation of w. The feasi' ility of achieving this desired control character depends primarily upon the wobble frequency p_1. As p_2 is increased, the response of w to an error signal containing Ω_x and Ω_y is diminished, and the required control torques can only be supplied by increasing the magnitude of u.

A similar (although lesser) problem arises when the torsional natural frequency p_2 is increased. However, the control logic which specifies $\zeta_2 = p_1/p_2$ largely eliminiates any difficulty in controlling the torsional motion by simply reducing the required damping factor as p_2 is increased. The following points concerning this procedure should be noted:

(a) As p_2 increases, the amplitudes of undamped torsional oscillations are reduced, and the influence of this mode of oscillation on the artificial-g environment in the crewquarters is reduced. Hence, the necessity for damping this mode of oscillation is reduced as p_2 increased.

(b) Attempts in this study to provide comp' ratively large damping factors (i.e., $.4 \leq \zeta_2 \leq .6$) for configurations having comparatively high values of p_2 were not notably successful in that a large control force ($u \cong 40$ lbs.) was required, and it was generally necessary to reduce the wobble damping rates ($.4 \leq \zeta_1 \leq .6$).

The results of all cases for $|u|_{max}$ and $|w|_{max}$ are summarized in Table 5.1 and 5.2. Table 5.1 contains the nominal ($\bar{\Omega}$ =4rpm.) cases for both the zero and finite torsional stiffness cases. The entries of 0 and 1 for deployment stages indicate the non-

deployed and fully-deployed cases, respectively. The overspin cases are summarized in TABLES 5.2.

TABLE 5.1(a): Transient performance for $\bar{\Omega}$ = 4 rpm., and k_t = 0.

Deployment Stage	$\|u\|_{max}$ (lb.)	$\|w\|_{max}$ (ft.)
0	15.9	16.2
1/4	19.0	16.5
1/2	9.7	16.1
3/4	19.1	16.5
1	14.2	16.5

TABLE 5.1(b): Transient performance for $\bar{\Omega}$ = 4 rpm., and $k_t > 0$.

Deployment Stage	$\|u\|_{max}$ (lb.)	$\|w\|_{max}$ (ft.)
0	15.9	16.2
1/4	15.8	16.5
1/2	12.1	14.9
3/4	13.8	15.7
1	16.1	16.3

TABLE 5.2(a): Transient performance for overspin cases with k_t = 0.

Deployment Stage	$\bar{\Omega}$(rpm.)	$\|u\|_{max}$ (lb.)	$\|w\|_{max}$ (ft.)
0	11.5	24.4	10.8
1/4	8.3	19.0	16.5
1/2	6.23	34.0	16.5
3/4	4.85	28.0	16.5
1	4.0	14.2	16.5

TABLE 5.2(b): Transient Performance for overspin cases with $k_t > 0$.

Deployment Stage	$\bar{\Omega}$(rpm.)	$\|u\|_{max}$ (lb.)	$\|w\|_{max}$ (ft.)
0	11.5	24.4	10.8
1/4	8.3	34.9	9.7
1/2	6.23	27.2	13.7
3/4	4.85	25.4	16.0
1	4.0	16.1	16.3

The results of these tables confirm the general conclusion of this study, namely, the MMC system can provide effective and generally satisfactory attitude stabilization for a wide range of space station configurations. In addition, the conclusions concerning specific parameter variations are as follows:

(a) Stage of Deployment. For a fixed spin velocity $\bar{\Omega}$, the changes in the stage of deployment have a comparatively minor direct in-influence on controller performance. This statement can be confirmed by inspecting Tables 5.1(a) and (b).

(b) Nominal spin velocity $\bar{\Omega}$. This is the single most important factor on system dynamics. In general, effective control is much more easily achieved for the nominal spin-velocity $\bar{\Omega}$ = 4 rpm. than the higher spin rates, which would suggest the advisability of spin-up or spin-down firings at the intermediate stages of deployment.

(c) Torsional stiffness k_t. In general, the MMC was equally effective for the k_t = 0 and McDonnell-Douglas designs. When k_t is zero, the torsional motion is uncontrollable, but has no effect on the crew quarter artificial-g environment. Furthermore, the gains k_t computed for k_t = 0 proved to be generally satisfactory for k_t up to 2000 ft.lb./rad. For the finite torsional stiffness cases, θ motion was coupled into the crew quarters, but the finite values of k_t enabled effective control of θ. During the course of this study, preliminary values for k_t were examined which were (erroneously) an order of magnitude larger than those cited in Section 4.4. However, gains were computed for these values (at

$\bar{\Omega}$ = 4 rpm for the fully-deployed configuration) which yielded an extremely effective control logic. At these elevated values the torsional frequency p_2 was much larger than the wobble frequency p_1, which in turn decreased and approached the rigid-body value $(ab)^{1/2}$. As noted previously, the control logic used in this study minimizes any control difficulties associated with large values for p_2.

In some cases where comparatively high wobble frequencies p_1 were encountered, a smaller value of control mass m_c = 7 slugs was employed in an attempt to lower the peak force magnitude $|u|_{max}$. The results were generally unsatisfactory, since this led to difficulties in satisfying the deflection constraint $|w| \leq 16.5$ ft.

5.2 EXTENSIONS

A logical sequel to this investigation would consist of a similar study with an improved dynamics model (such as that proposed by Nixon) for cable-connected configurations. An improved dynamics model would include the complete rotational degrees of freedom for crewquarters and counterweight, but would not require extensional motion between the bodies. The control logic and synthesis procedure employed in this study should apply for an improved model, since basically only an increase in dimensionality is involved.

Several practical problems which would arise in the implementation of an MMC system remain unresolved. For example, the proper technique for measuring system variables (θ, $\dot{\theta}$, etc.) is not clear. Furthermore, while the physical requirements of an MMC system would seem to be modest, a hardware investigation with the

objective of fabricating and testing an MMC tc establish its operating characteristics would be of considerable value.

REFERENCES

1. Childs, D.W., "A Movable-Mass Attitude Stabilization System for Artificial-G Spacestations," Journal of Spacecraft and Rockets, Vol. 8, No. 8, August, 1971, pp. 829-834.
2. Austin, F., "Nonlinear Dynamics of a Free-Rotating Flexibly Connected Double-Mass Space Station," Journal of Spacecraft and Rockets, Vol. 2, No. 6, Nov.-Dec. 1965, pp. 901-906
3. Crist, S.A., and Eisley, J.G., "Motion and Stability of a Spinning Spring-Mass System in Orbit," Journal of Spacecraft and Rockets, Vol. 6, No. 7, July, 1969, pp. 819-824.
4. Tai, C.L. and Loh, M.M.H., "Planar Motion of a Rotating Cable-Connected Space Station in Orbit," Journal of Spacecraft and Rockets, Vol. 2, No. 6, Nov.-Dec., 1965, pp. 889-894
5. Chobotov, V., "Gravity-Gradient Excitation of a Rotating Cable-Counterweight Space Station in Orbit," Journal of Applied Mechanics, Vol. 30, No. 4, Dec. 1963, pp. 547-554.
6. Stabekis, P. and Bainum, P.M., "Motion and Stability of a Rotating Space Station-Cable-Counterweight Configuration," Journal of Spacecraft and Rockets, Vol. 7, No. 8, Aug. 1970, pp. 912-918.
7. Posnansky, H.A. and Heeschen, C.M.,Jr., Dynamics of an Elastic Space Station, Final Report April 1970, Contract NAS8-24768, Lockheed Missiles and Space Company, Huntsville Research and Engineering Center, Huntsville Research Park, 4800 Bradford Drive, Huntsville, Alabama.
8. McDonnell Douglas Astronautics Company-West, Space Station Definition, Volume IV, Configuration Analysis, Contract NAS8-25140,

MSFC-DRL-160 Line Item 8, July 1970.

9. Nixon, D.D., Dynamics of a Spinning Space Station with a Counterweight Connected by Multiple Cables, AIAA Paper No. 72-172, AIAA 10th Aerospace Sciences Meeting, San Diego, California/ January 17-19, 1972.

APPENDIX A: Closed-Loop Characteristic Polynomial

The closed-loop polynomial, which is obtained by an expansion of the determinant $|sI-A-bk^T|$, is of the form

$$s^7 + \alpha_6 s^6 + \alpha_5 s^5 + \alpha_4 s^4 + \alpha_3 s^3 + \alpha_2 s^2 + \alpha_1 s^1 + \alpha_0 = 0 \qquad (A.1)$$

where each of the α_i's is a linear function of the unknown gains k_i, i.e.,

$$\alpha_i = c_i + \sum_{j=1}^{6} \alpha_{ij} k_j \qquad (A.2)$$

From Eq. (26), the α_{ij} coefficients were determined as follows:

α_6: $\alpha_{61} = (r_y/I_x)$, $\alpha_{63} = -\alpha_{62} = (r_x/I_y)$

$\alpha_{64} = \alpha_{66} = 0$, $\alpha_{65} = -(1 + e_1)/m_c$, $\alpha_{67} = 0$

α_5: $\alpha_{51} = \bar{\Omega}\, \alpha_{63} [a + e(1 - b_2)]$

$\alpha_{52} = \bar{\Omega}\, \alpha_{61} b_1$, $\alpha_{53} = \alpha_{61}(b_2 - b_1)$

$\alpha_{54} = \alpha_{63}$, $\alpha_{55} = 0$, $\alpha_{56} = \alpha_{65}$, $\alpha_{57} = 0$

α_4: $\alpha_{41} = \alpha_{61} [\bar{\Omega}^2 (1 + b_2) + P_1^2]$

$\alpha_{42} = \alpha_{63} [-\bar{\Omega}^2 (1 + b_2 + eb_2^2 - eb_2) - (k_t/I_y^2)]$

$\alpha_{43} = \bar{\Omega}^2\, \alpha_{63} (1 + ab_2)$

$\alpha_{44} = \bar{\Omega}\, \alpha_{61} (b_2 - b_1)$

$\alpha_{45} = -(1/m_c + r_y \alpha_{61}) P_1^2$

$+ (\bar{\Omega}^2/m_c)\{e(1-b_2)(b_2 - b_1) - ab_1 - b_2)\}$

$- \bar{\Omega}^2\, r_y\, \alpha_{61} (b_1 + b_2)$

$- \bar{\Omega}^2\, r_x\, \alpha_{63} \{a + e\,(1 - b_2)^2 - b_2 - k_t/(I_y^2\, \Omega^2)\}$

$\alpha_{46} = 0$, $\alpha_{47} = \alpha_{56}$

α_3: $\alpha_{31} = \bar{\Omega}\,\alpha_{53}\,\{\bar{\Omega}^2[a(1+b_2)+e(1-b_2)]+(ak_t/I_y^2)\}$

$\alpha_{32} = \bar{\Omega}\,\alpha_{61}\,\{\bar{\Omega}^2 b_1(1+b_2) + k_t(b_2/I_y^1 + b_1/I_y^2)\}$

$\alpha_{33} = \bar{\Omega}\,\alpha_{44}$, $\alpha_{34} = \alpha_{43}$, $\alpha_{35} = 0$

$\alpha_{36} = \alpha_{45} + 2(1/m_c + r_y\alpha_{61})P_1^2$

$\alpha_{37} = \alpha_{46} = 0$,

α_2: $\alpha_{21} = \bar{\Omega}^2\,\alpha_{61}\,(\bar{\Omega}^2 b_2 + P_1^2)$

$\alpha_{22} = \bar{\Omega}^2\,\alpha_{63}\,\{\bar{\Omega}^2[eb_2(1-b_2) - b_2] - (I_t/I^2_y)]$

$\alpha_{23} = \bar{\Omega}^4\,\alpha_{63}\,ab_2$, $\alpha_{24} = \alpha_{33}$, $\alpha_{26} = 0$

$\alpha_{25} = \bar{\Omega}^2 a(1-b_2)\,r_x\,\alpha_{63}$

$-\bar{\Omega}^2(a/m_c + r_y\alpha_{61})\,\{k_t(b_2/I^1_y + b_1/I^2_y) + \bar{\Omega}^2 b_1 b_2\}$

$\alpha_{27} = \alpha_{36}$

α_1: $\alpha_{11} = \bar{\Omega}^3\,a\alpha_{63}\,(\bar{\Omega}^2\,b_2 + k_t/I^2_y)$

$\alpha_{12} = \bar{\Omega}^3\,\alpha_{61}\{\bar{\Omega}^2 b_1 b_2 + k_t(b_2/I^1_y + b_1/I^2_y)\}$

$\alpha_{13} = 0$, $\alpha_{14} = -\bar{\Omega}^4 ab_2\,\alpha_{63}$, $\alpha_{15} = 0$

$\alpha_{16} = \alpha_{25}$, $\alpha_{17} = 0$

α_0: $\alpha_{01} = \alpha_{02} = \alpha_{03} = \alpha_{04} = \alpha_{05} = \alpha_{06} = 0$, $\alpha_{07} = \alpha_{16}$

The c_i coefficients are:

$c_6 = c_4 = c_2 = 0$

$c_5 = -\bar{\Omega}^2\{e(1-b_2)(b_2 - b_1) + e_1\}$

$c_3 = \bar{\Omega}^2 ab_2(k_t/I^1_y) + (\bar{\Omega}^2 b_2 + k_t/I^2_y)(\bar{\Omega}^2 ab_1 - e_1)$

$-m_c\bar{\Omega}^4\{b_1 r_y\alpha_{61} + ar_x\alpha_{63} - r_x\,e(1-b_2)^2\alpha_{63}\}$

$-m_c\bar{\Omega}^2 r_y\,\alpha_{61}\,k_t/I^1_y$

$c_1 = m_c\bar{\Omega}^4\,\{(b_2\bar{\Omega}^2 + k_t/I_y^2)(b_1 r_y\alpha_{61} + ar_x\alpha_{63})$

$+r_y b_2\alpha_{61}\,k_t/I^1_y\}$